

1 Luminescence and a New Approach for Detecting Heat 2 Treatment of Geuda Sapphire

3
4 Teerarat Pluthametwisute^{1,2}, Lutz Nasdala², Chutimun Chanmuang N.², Manfred Wildner², Eugen
5 Libowitzky², Gerald Giester², E. Gamini Zoysa³, Chanenkant Jakkawanvibul⁴, Waratchanok
6 Suwanmanee⁴, Tasnara Sripoonjan⁵, Thanyaporn Tengchaisri⁶, Bhuwadol Wanthanachaisaeng⁴
7 and Chakkaphan Sutthirat¹
8

9 ¹Department of Geology, Faculty of Science, Chulalongkorn University, 10330 Bangkok, Thailand;

10 ²Institut für Mineralogie und Kristallographie, Universität Wien, 1090 Wien, Austria;

11 ³Mincraft Co., 10370 Mount Lavinia, Sri Lanka;

12 ⁴The Gem and Jewelry Institute of Thailand (Public Organization), 10500 Bangkok, Thailand;

13 ⁵G-ID Laboratories, Bangkok, 10120, Thailand;

14 ⁶Science and Technology Park (STeP), Chiang Mai University, 50200 Chiang Mai, Thailand.
15

16 **Correspondence:** Chakkaphan Sutthirat (email: chakkaphan.s@chula.ac.th)
17

18 **Abstract.** For decades, unravelling heat treatment of sapphire has been a challenging issue. The present
19 study offers new aspects that support the detection of heat treatment of sapphire. Natural unheated geuda
20 sapphire exhibits orange to red luminescence under long-wave ultraviolet (LWUV, 365 nm) light, while
21 heated geuda sapphire shows blue luminescence under short-wave ultraviolet (SWUV, 225 nm). Natural
22 unheated sapphire is distinguishable from heated sapphire by its orange to red luminescence under long-
23 wave ultraviolet (LWUV, 365 nm) light, whereas blue luminescence under short-wave ultraviolet (SWUV,
24 254 nm) light indicates their heated counterparts. Light, UV-excited photoluminescence reveals a connection
25 between the broad emission spectrum of natural unheated sapphire, which appears orange to red under
26 LWUV illumination, and the emission spectrum of heated sapphire, which appears blue under SWUV
27 illumination. UV-excited photoluminescence shows a linkage between a broad emission spectrum within
28 the orange to red region and orange to red luminescence of natural unheated sapphire under LWUV
29 illumination, as well as an emission spectrum around the green region and blue luminescence of heated
30 sapphire under SWUV illumination. The presence of melt inclusions in dissolved silks serves as an indicator
31 of sapphire heat treatment. Fourier-transform infrared (FTIR) spectroscopy alone is insufficient for
32 distinguishing unheated from heated sapphire. By combining orange to red luminescence with blue
33 luminescence and melt inclusions, we provide a practical method for accurately differentiating natural gem-
34 quality sapphire and heated gem-quality sapphire. Furthermore, the presence of melt inclusions within
35 dissolved silks may be used as an indicator of heat treatment of sapphire. It seems that Fourier-transform
36 infrared (FTIR) spectroscopy alone is inadequate for distinguishing unheated and heated sapphire. The
37 application of orange to red, and blue luminescence together with melt inclusions offer a novel and
38 practicable procedure for more precise differentiation of unheated versus heated sapphire.

39
40 Keywords: gem; sapphire; heat treatment; luminescence

41
42 **1 Introduction**
43

44 Since the 1970s, Sri Lanka has been renowned for its gemstone resources, particularly geuda sapphire, a
45 milky or silky corundum variety that is frequently heat-treated to enhance color and clarity (Soysa and
46 Fernando, 1992; Ediriweera and Perera, 1989; Perera et al., 1991). High-temperature treatment of
47 corundum (including ruby and sapphire) can significantly alter its milkiness, asterism, color, and internal
48 features such as mineral inclusions (Nassau, 1981; Ediriweera and Perera, 1989; Hughes, 1997, 2017; Kvi
49 et al., 1999; Pisutha-Arnond, 2017; Themelis, 2018). Key factors in these transformations include the
50 temperature, duration, and atmospheric conditions of the heating process (Nassau, 1981; Emmett and
51 Douthit, 1993; Peiris, 1993; Emmett et al., 2003; Hughes, 2017; Pisutha-Arnond, 2017; Soonthorntantikul
52 et al., 2019).
53 One of the first-rank challenges encountered by gemologists nowadays is the precise and reliable
54 identification of heat-treated ruby and sapphire. Blue luminescence under SWUV light, observed in heated
55 sapphire for over 50 years (Crowningshield 1966, 1970), can extend into the green region (Nassau, 1981)
56 and has been extensively studied (Evans, 1994; Wong et al., 1995a; Wong et al., 1995b; Hughes 1997;
57 McClure and Smith, 2000; Page et al., 2010; Alombert-Goget et al., 2016a; Alombert-Goget et al., 2016b;
58 Hughes, 2017; Vigier et al., 2021a, b, 2023). ~~Since the 1970s, Sri Lanka has maintained an outstanding~~
59 ~~record for its rich supply of gemstones (Soysa and Fernando, 1992). Among diverse corundum varieties,~~
60 ~~the so-called geuda sapphire is noteworthy, as it has been often subjected to high-temperature heat treatment~~
61 ~~to increase its value by enhancement of color and clarity (Ediriweera and Perera, 1989; Perera et al., 1991).~~
62 ~~Geuda sapphire is characterized by milky and/or silky appearance. Heat treatment of corundum (ruby and~~
63 ~~sapphire) has the capacity to modify the appearance of milkiness and asterism, color, and even the internal~~
64 ~~features (including mineral inclusions) of the gemstones. Blue luminescence under SWUV light, observed~~
65 ~~in heated sapphire for over 50 years (Crowningshield 1966, 1970), can extend into the green region~~
66 ~~(Nassau, 1981) and has been extensively studied (Evans, 1994; Wong et al., 1995a; Wong et al., 1995b;~~
67 ~~Hughes 1997; McClure and Smith, 2000; Page et al., 2010; Alombert-Goget et al., 2016a; Alombert-Goget~~
68 ~~et al., 2016b; Hughes, 2017; Vigier et al., 2021a, b, 2023).~~ This luminescence may relate to rutile inclusions
69 commonly found in natural blue sapphire (Hughes, 2017). During heating at around 1600 °C, rutile
70 decomposes, incorporating Ti⁴⁺ ions into the sapphire structure (Sutthirat et al., 2006). Blue luminescence
71 serves as a key indicator of heat treatment in sapphire (Crowningshield, 1966; McClure and Smith, 2000;
72 Hughes, 2017; Hughes and Perkins, 2019). However, changes in original brown silk inclusions and orange
73 luminescence in natural unheated sapphire, relative to blue luminescence in heated sapphire, have not been
74 thoroughly explored. ~~Temperature and duration of the heating process, as well as reducing or oxidizing~~
75 ~~conditions, are the most significant factors influencing corundum's alterations (Nassau, 1981; Emmett and~~
76 ~~Douthit, 1993; Peiris, 1993; Emmett et al., 2003; Hughes, 2017; Pisutha-Arnond, 2017; Soonthorntantikul~~
77 ~~et al., 2019). Heat treatment can be classified as high- or low-temperature according to the decomposition~~
78 ~~of rutile silks in corundum (Nassau, 1981; Emmett and Douthit, 1993; Emmett et al., 2003; Hughes, 2017;~~

Hughes and Perkins, 2019). The term low-temperature heat treatment has been used (typically referred to as below 1000 °C) when rutile particles still reveal their original structures. On the other hand, temperatures beyond 1350 °C denote high-temperature heat treatment when rutile silks start to decompose and dissolve within the corundum host (Hughes, 2017; Themelis, 2018). Consequently, internal diffusion (indicated by a colored halo surrounding the crystal inclusion), molten or altered inclusions, and/or broken silk are strong indicators of high-temperature heat treatment. However, low-temperature heat treatment can also produce various altered mineral inclusions (Kammerling et al., 1990; McClure and Smith, 2000; McClure et al., 2010; Pisutha-Arnond, 2017; Soonthorntantikul et al., 2019).

The present study provides a novel approach by observing the transformations in silk inclusions and luminescence in sapphire before and after heating. ~~One of the first-rank challenges encountered by gemologists nowadays is the precise and reliable identification of heat-treated ruby and sapphire. Blue luminescence under SWUV light has been observed in heated sapphire some 50 years ago (Crowningshield 1966, 1970). This luminescence may also extend into the green region (Nassau, 1981). It has been studied afterwards by numerous researchers (Evans, 1994; Wong et al., 1995a; Wong et al., 1995b; Hughes 1997; McClure and Smith, 2000; Page et al., 2010; Alombert-Goget et al., 2016a; Alombert-Goget et al., 2016b; Hughes, 2017; Vigier et al., 2021a, b, 2023). This phenomenon may relate to rutile inclusions in sapphire (Hughes, 2017). It should be mentioned that most natural blue sapphires contain some exsolved rutile (TiO₂) in the form of silk and/or needle inclusions (Sutthirat et al., 2006; Hughes, 2017). When these sapphire samples are heated, rutile dissolves gradually at temperatures of about 1600 °C (Sutthirat et al., 2006), resulting in the incorporation of Ti⁴⁺ ions into the host sapphire structure. After Ti⁴⁺ being exposed to SWUV light, they yield luminescence. However, blue luminescence was not observed in both unheated and heated basaltic sapphire, possibly due to the abundant presence of Fe²⁺ of basaltic origin that may strongly quench such blue luminescence (Soonthorntantikul et al., 2019). More details will be discussed in this report. Furthermore, even though microscopic inclusions have been the distinguishing characteristics of heated sapphire, identifying heat-treated sapphire remains challenging (Crowningshield, 1966; Hughes, 2017). Spectroscopic techniques such as Fourier transform infrared (FTIR) spectroscopy have also been applied to detect heated sapphire. In some cases, the presence or absence of specific FTIR features in the O-H absorption region (3100–3600 cm⁻¹) may serve as an indicator of heat treatment (Smith, 1995; Beran and Rossman, 2006; Saesaw et al., 2018); however, it is probably not a conclusive evidence (Ediriweera and Perera, 1989; Perera, 1993; Sutthirat et al., 2006; Cartier, 2009; Jaliya et al., 2020). The most efficient technique and key evidence enabling to identify heat-treated sapphire is its blue luminescence (Crowningshield, 1966; McClure and Smith, 2000; Hughes, 2017; Hughes and Perkins, 2019). However, sequential research on original brown silk inclusions and orange luminescence in natural unheated sapphire in relation with blue luminescence in the heated counterparts has never been reported accordingly. Therefore, this study should be the first research that represents an innovative approach to observe both original silk inclusions and luminescence in sapphire and their change after heating experiments.~~

2 Materials and Methods

118 ~~Natural unheated geuda sapphire (A-type) samples (types of samples, see as described by Vertriest et al.,~~
119 ~~2019) were separated based on the appearance of silk inclusions into three distinctive groups, i.e., high-~~
120 ~~density-silk (HS), low-density-silk (LS), and silk-free (SF) specimens. Natural unheated geuda sapphire~~
121 ~~samples were separated into 3 groups: (Fig. 1-1) high-density-silk group; 2) low-density-silk group; and 3)~~
122 ~~silk-free group (Fig. 1-).~~ Using an Enraf-Nonius Kappa single-crystal X-ray diffractometer (sXRD)
123 with a ~~charge-coupled device (CCD)~~ area detector, these samples were oriented (based on 10 frames at a
124 crystal detector distance of 35 mm), cut and polished into wafers with surfaces parallel to the *c*-axis.
125 ~~For chemical analysis using an~~ electron probe micro-analyser (EPMA) ~~system,~~ slabs were coated
126 with carbon for conductivity.

127 Heating experiments were conducted using a high-temperature electric furnace, Linn-
128 HT-1800-Vac. Heating was performed under ambient atmospheric conditions without any additional
129 oxygen buffer. Experimental conditions involved the maximum temperature of 1650 °C, which was
130 maintained for 10 hours, prior to natural cooling down in the furnace. A heating rate of 300 °C per hour
131 was set to reach the maximum temperature. To minimize surface contamination, the samples were placed
132 into a highly purified alumina (Al₂O₃) crucible.

133 ~~Basic gemological data, such as-~~The refractive index, ~~of samples~~ was measured by a
134 gemological refractometer (KRUSS, model ER605) with 1.81 refractive index liquid. Specific gravity was
135 determined by a hydrostatic weighing balance, ~~by weighing samples in water (with a drop of dishwashing~~
136 ~~detergent added to reduce surface tension) and in air.~~

137 Micro-inclusions in all samples were ~~investigated~~ imaged using an Olympus BX-series
138 microscope equipped with Olympus DP27 digital camera. The camera was operated using the Olympus
139 Stream micro-imaging software. Raman spectra of inclusions were acquired using a confocal micro-
140 Raman spectrometer Horiba Jobin Yvon LabRAM-HR Evolution. Using 473 nm laser excitation (15 mW
141 at the sample) and a 50×/0.50 objective lens, a spectral range of 100–1350 cm⁻¹ Raman shift was recorded.
142 Wavenumber calibration was done using the Rayleigh line, resulting in wavenumber accuracy of better
143 than 0.5 cm⁻¹. A spectral resolution of ca. 1.2 cm⁻¹ resulted from 800 mm focal length and an 1800
144 grooves/mm optical grating in the monochromator system. For more details see Zeug et al. (2018).

145 Chemical compositions of the samples were determined using a JEOL JXA 8100 EPMA.
146 Analytical conditions were set to 15 kV accelerating voltage and a probe current of about 2.5×10^{-8} A with
147 electron beam focussed to <1 μm. Natural mineral and synthetic oxide references were selected suitably
148 for calibration, including fayalite (Fe₂SiO₄) for Fe, wollastonite (CaSiO₃) for Ca, synthetic corundum
149 (Al₂O₃) for Al, synthetic periclase (MgO) for Mg, synthetic quartz (SiO₂) for Si, potassium titanyl
150 phosphate (KTiOPO₄) for K and Ti, synthetic manganosite (MnO) for Mn, synthetic eskolaite (Cr₂O₃) for
151 Cr, synthetic gadolinium gallium garnet (Gd₃Ga₅O₁₂) for Ga, and synthetic lead vanadium germanium
152 oxide for V. Counting times were 600 s peak and 300 s background for all elements. The K-α line was
153 analysed for all elements except for Ga where the L-α line was measured. Analytical crystals were selected
154 appropriately including thallium acid phthalate (TAP) crystal for Si and Al; pentaerythriol (PET) crystal
155 for Ti, Mg, K, and Ca; lithium fluoride (LiF) crystal for V, Cr, Ga, Fe, and Mn. The detection limit

156 (estimated from threefold background noise) is approximated at 0.005 wt% or 50 ppm. Three analytical
157 spots in each sample were selected for further analysis analyzed.

158 Polarized optical absorption (UV-VIS-NIR) spectra of samples were recorded on
159 double-sided polished crystal slabs in the spectral range of 35000–3500 cm⁻¹, covering the near
160 ultraviolet (UV), the visible (VIS) and the near infrared (NIR) ranges. The measurements were performed
161 in the sample chamber of a Bruker Vertex 80 FTIR spectrometer at 2 mm measuring spot, using a calcite
162 Glan-prism polarizer and appropriate combinations of light sources (Xe or W lamp), beam splitters (CaF₂-
163 VIS/UV or CaF₂-NIR), and detectors (GaP, Si or InGaAs diodes) to cover the desired spectral
164 range. Hence, each full spectrum was combined from three partial spectra: 1) 35000–18000 cm⁻¹ with 40
165 cm⁻¹ spectral resolution and averaged from 256 scans; 2) 18000–9500 cm⁻¹ with 20 cm⁻¹ resolution and
166 256 scans; 3) 9500–3500 cm⁻¹ with 10 cm⁻¹ resolution and 128 scans.

167 Fourier-transform infrared (FTIR) spectra were acquired by means of a Bruker Tensor
168 27 FTIR spectrometer attached to a Bruker Hyperion microscope in the spectral range from 4000 cm⁻¹ to
169 1600 cm⁻¹. A glowbar light source, a KBr beamsplitter, and a deuterated L-alanine doped triglycene
170 sulphate (dLATGS; Tensor27) or Hg-Cd-telluride (MCT) detector (Hyperion) were employed. The
171 spectral resolution was 4 cm⁻¹, sample and reference spectra were averaged from 128 scans.

172 Luminescence phenomena were observed and photo-captured both before and after heat
173 treatment. The images were obtained under LWUV (365 nm) illumination using ZEISS microscope model
174 stemi 508 with 0.63x magnification. The images were captured in a darkened room using CANON digital
175 single lens reflex (DSLR) camera model EOS 80D (24.2 MP resolution), which was mounted on top of the
176 microscope. The SUPERFIRE UV (365 nm) mini flashlight model S11-H, 3W (max), DC 3.7 V, was held
177 approx. 15 cm above the samples. The camera settings involved an exposure time of 5 seconds, an exposure
178 bias of 0 steps, and an ISO speed of 200. The aperture was adjusted to f/0, and the focal length of 0 nm.
179 commercial UV lamp, and For under-SWUV (254 nm) illumination (approximately 225 nm), by means of
180 a DiamondView™ device (approx. 225 nm) was used. The parameter settings for DiamondView™
181 were established as follows: Integration duration: 2.83 seconds; minimum excitation status: Off. Power
182 settings ranged from 50% to 80%, contingent upon the intensity of luminescence. A gain of 13.85 dB is
183 measured. We set the aperture was set to 80% and the field stop to 67%. Gamma was disabled.

184 Photoluminescence (PL) spectra in the visible and NIR ranges were acquired using a confocal
185 Horiba Jobin Yvon LabRAM-HR 800 spectrometer. Spectra were excited using the 325 nm emission of a
186 He-Cd laser (ca. 10 mW at the sample surface). The system was calibrated using emission lines of a Kr
187 lamp. The spectral resolution was in the range 0.07 nm (violet) to 0.02 nm (NIR range).

188 All the spectra were acquired at the same position both before and after heating
189 experiments.

190

191 3 Results

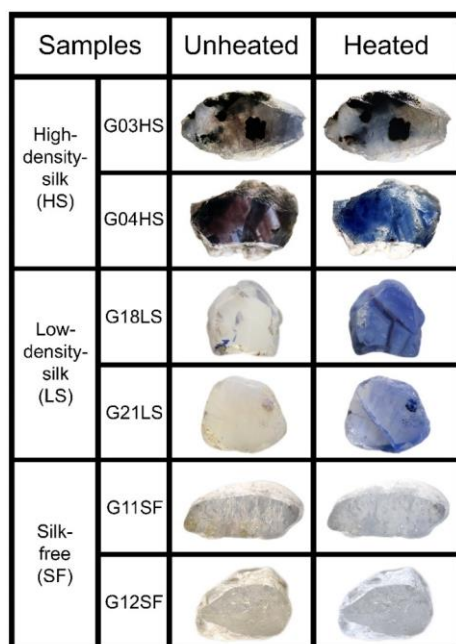
192

193 3.1 Heating-induced property changes and alteration

194 Natural unheated geuda sapphire samples were separated based on the appearance of silk inclusions into

195 three distinctive groups, i.e., high-density-silk, low-density-silk, and silk-free specimens. Representatives
 196 of natural unheated and their heated counterparts of all groups are shown in Fig. 1. All the samples ranged
 197 from a specific gravity of 3.83 to 4.08 g/cm^3 , and refractive indices of 1.760 to 1.770 falling well within
 198 the field-range of corundum's properties. Before heating, samples showed varying natural appearances
 199 based on inclusion density. Geuda samples with HS inclusions (e.g., G03HS and G04HS, Fig. 1) exhibited
 200 brown silk and brown color banding or zoning, while a few samples also displayed a natural blue color.
 201 Samples with LS inclusions (e.g., G18LS and G21LS, Fig. 1) generally appeared milky with yellowish or
 202 brownish tints. After heating, most samples turned blue, ranging from pale to dark shades, with the milky
 203 appearance and yellowish or brownish tints significantly reduced. After heating, most samples turned blue,
 204 varying from pale blue to dark blue. Alteration was clearly observed in the geuda samples with high-
 205 density-silk inclusions (G03 and G04, Fig. 1), which naturally showed brown silk and brown color
 206 banding/zoning. Moreover, a few samples in this group also showed a natural blue appearance (G02, Fig.
 207 8). Regarding sapphire samples with low-density-silk inclusions, these stones (e.g., G18 and G21, Fig. 1)
 208 typically presented a milky appearance with yellowish or brownish tints, which were obviously diminished
 209 after heating. On the other hand, the silk-free SF group usually showed a slightly yellowish appearance (Fig.
 210 1, samples G11SF and G12SF). After the heating experiment, they had changed slightly to a very pale blue
 211 color.

212



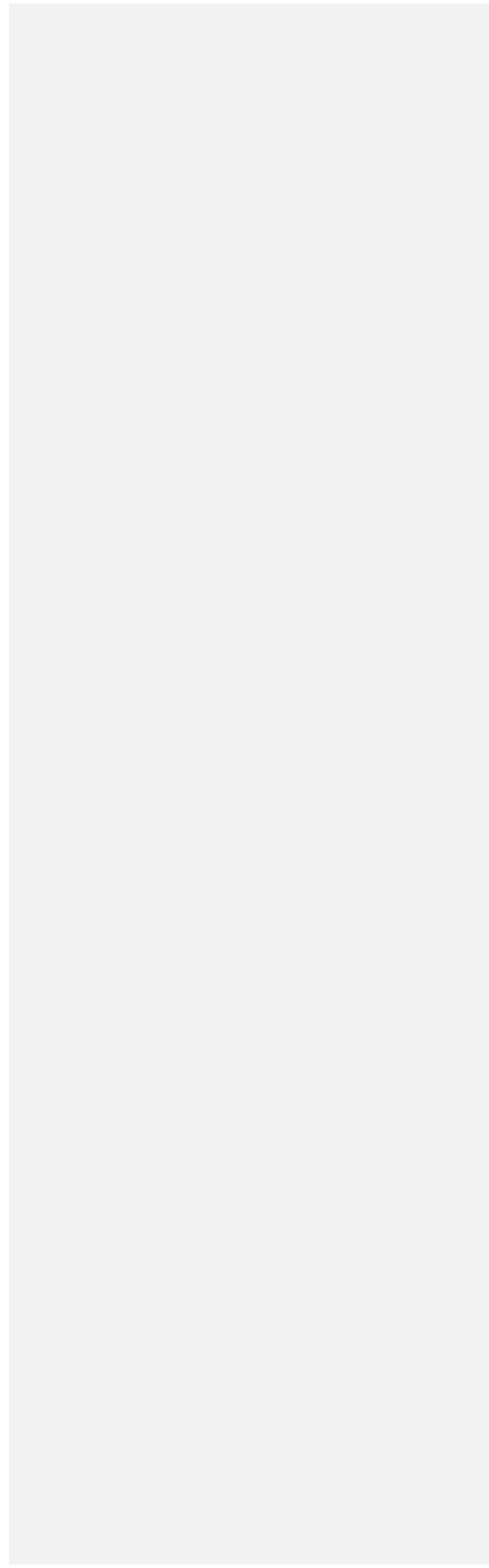
213

214 **Figure 1.** Representatives of natural unheated geuda sapphire samples within three separate groups, i.e.,
 215 HS (G03HS, G04HS), LS (G18LS, G21LS), and SF (G11SF, G12SF) groups, and their appearances after
 216 heating. Sizes of stones range between 0.44 and 12 mm.

217

218 3.2 Mineral chemistry

219 Chemical compositions of samples in the three distinct groups are summarized in Tables 1 to 3. The Al_2O_3
220 contents range between 98.2 and 99.5 wt%. Other elements are found as trace contents only, particularly
221 Fe, Ti, and Ga. Fe and Ti are essential coloring elements in sapphire. The ~~high-density-silk~~**HS** group
222 contained the highest Fe contents of 0.32–0.36 wt% FeO, together with 0.02–0.04 wt% TiO_2 and <0.7
223 wt% Ga_2O_3 . The ~~low-density-silk~~**LS** group had a high Ti content of 0.02–0.51 wt% TiO_2 with ≤ 0.06 wt%
224 FeO and ≤ 0.8 wt% Ga_2O_3 . The ~~silk-free~~**SF** group contained 0.06–0.26 wt% FeO, ≤ 0.04 wt% TiO_2 and <1
225 wt% Ga_2O_3 . The general detection limits of major and minor analyses obtained from EPMA analyses are
226 typically roughly estimate at 50 ppm.



228 **Table 1.** Representative chemical compositions (EPMA results) and calculated mineral formulae of [high-](#)
 229 [density-silkHSHS sapphire samples](#)[sapphire samples](#).

Samples	G01HS	G02HS	G03HS	G04HS
Major oxides (wt%):				
SiO ₂	0.00	0.00	0.45	0.40
TiO ₂	0.02	0.02	0.04	0.03
Al ₂ O ₃	99.0	98.7	98.9	98.7
V ₂ O ₃	0.01	0.00	0.00	0.03
Cr ₂ O ₃	0.00	0.02	0.03	0.00
Ga ₂ O ₃	0.62	0.66	0.00	0.39
FeO _{total} *	0.32	0.33	0.36	0.36
MnO	0.02	0.00	0.00	0.02
MgO	0.00	0.00	0.01	0.01
K ₂ O	0.00	0.00	0.00	0.00
CaO	0.01	0.01	0.02	0.01
Total	100.0	99.8	99.8	100.0
Mineral formulae (apfu)**:				
Si	0.000	0.000	0.008	0.007
Ti	0.000	0.000	0.001	0.000
Al	1.990	1.989	1.985	1.982
V	0.000	0.000	0.000	0.000
Cr	0.000	0.001	0.000	0.000
Ga	0.007	0.007	0.000	0.004
Fe	0.013	0.014	0.005	0.005
Mn	0.000	0.000	0.000	0.000
Mg	0.000	0.000	0.000	0.000
K	0.000	0.000	0.000	0.000
Ca	0.000	0.000	0.000	0.000
Sum	2.010	2.011	1.999	2.000

230 * FeO_{total} = total Fe oxide, assuming all Fe to be ferrous

231 ** Calculated based on 3 O atoms per formula unit

232

233 **Table 2.** Representative chemical compositions (EPMA results) and calculated mineral formulae of ~~low-~~
 234 ~~density-silk sapphire samples.~~ LS sapphire samples.

Samples	<u>G06LS</u>	<u>G16LS</u>	<u>G18LS</u>	<u>G20LS</u>	<u>G21LS</u>
Major oxides (wt%):					
SiO ₂	0.00	0.00	0.11	0.00	0.00
TiO ₂	0.04	0.27	0.37	0.51	0.02
Al ₂ O ₃	99.0	98.5	98.4	98.3	98.6
V ₂ O ₃	0.02	0.03	0.01	0.02	0.01
Cr ₂ O ₃	0.00	0.06	0.00	0.02	0.00
Ga ₂ O ₃	0.10	0.37	0.58	0.81	0.59
FeO _{total} *	0.00	0.06	0.06	0.06	0.05
MnO	0.01	0.00	0.00	0.00	0.01
MgO	0.02	0.02	0.01	0.01	0.02
K ₂ O	0.00	0.00	0.00	0.00	0.00
CaO	0.00	0.00	0.01	0.01	0.00
Total	99.2	99.3	99.6	99.7	99.3
Mineral formulae (apfu)**:					
Si	0.000	0.000	0.002	0.000	0.000
Ti	0.001	0.003	0.005	0.007	0.000
Al	1.997	1.989	1.984	1.981	1.992
V	0.000	0.000	0.000	0.000	0.000
Cr	0.000	0.002	0.000	0.001	0.000
Ga	0.001	0.004	0.006	0.009	0.007
Fe	0.000	0.002	0.002	0.002	0.002
Mn	0.000	0.000	0.000	0.000	0.000
Mg	0.001	0.001	0.001	0.000	0.001
K	0.000	0.000	0.000	0.000	0.000
Ca	0.000	0.000	0.000	0.000	0.000
Sum	2.001	2.003	2.000	2.000	2.002

235 * FeO_{total} = total Fe oxide, assuming all Fe to be ferrous

236 ** Calculated based on 3 O atoms per formula unit

237

238 **Table 3.** Representative chemical compositions (EPMA results) and calculated mineral formulae of ~~silk-~~
 239 ~~free sapphire samples~~, **SF sapphire samples**.

Samples	G07SF	G11SF	G12SF	G14SF	G22SF	G23SF
Major oxides (wt%):						
SiO ₂	0.01	0.13	0.06	0.00	0.00	0.00
TiO ₂	0.03	0.04	0.03	0.00	0.04	0.01
Al ₂ O ₃	98.7	98.7	98.8	99.5	98.2	98.7
V ₂ O ₃	0.00	0.02	0.00	0.00	0.00	0.00
Cr ₂ O ₃	0.00	0.00	0.01	0.00	0.00	0.00
Ga ₂ O ₃	0.71	0.00	0.00	0.15	0.78	0.94
FeO _{total} *	0.06	0.26	0.08	0.10	0.22	0.13
MnO	0.01	0.02	0.00	0.01	0.02	0.00
MgO	0.00	0.02	0.00	0.00	0.00	0.00
K ₂ O	0.00	0.01	0.00	0.00	0.00	0.00
CaO	0.02	0.00	0.02	0.01	0.01	0.01
Total	99.6	99.2	99.0	99.8	99.3	99.8
Mineral formulae (apfu)**:						
Si	0.000	0.002	0.001	0.000	0.000	0.000
Ti	0.000	0.001	0.000	0.000	0.001	0.000
Al	1.991	1.993	1.997	1.997	1.988	1.988
V	0.000	0.000	0.000	0.000	0.000	0.000
Cr	0.000	0.000	0.001	0.000	0.000	0.000
Ga	0.008	0.000	0.000	0.002	0.009	0.010
Fe	0.002	0.011	0.003	0.004	0.009	0.005
Mn	0.000	0.000	0.000	0.000	0.000	0.000
Mg	0.000	0.001	0.000	0.000	0.000	0.000
K	0.000	0.000	0.000	0.000	0.000	0.000
Ca	0.000	0.000	0.000	0.000	0.000	0.000
Sum	2.002	2.009	2.003	2.003	2.007	2.004

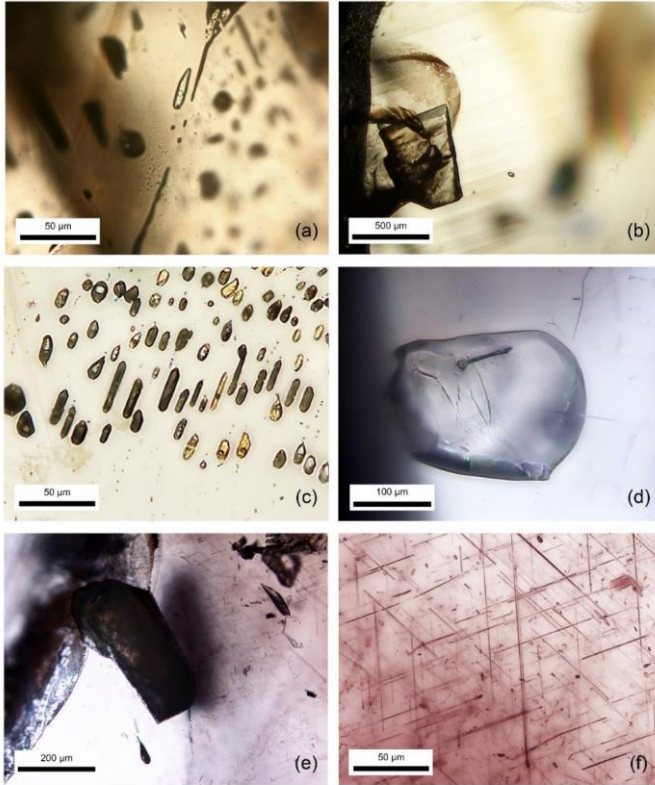
240 * FeO_{total} = total Fe oxide, assuming all Fe to be ferrous

241 ** Calculated based on 3 O atoms per formula unit

242

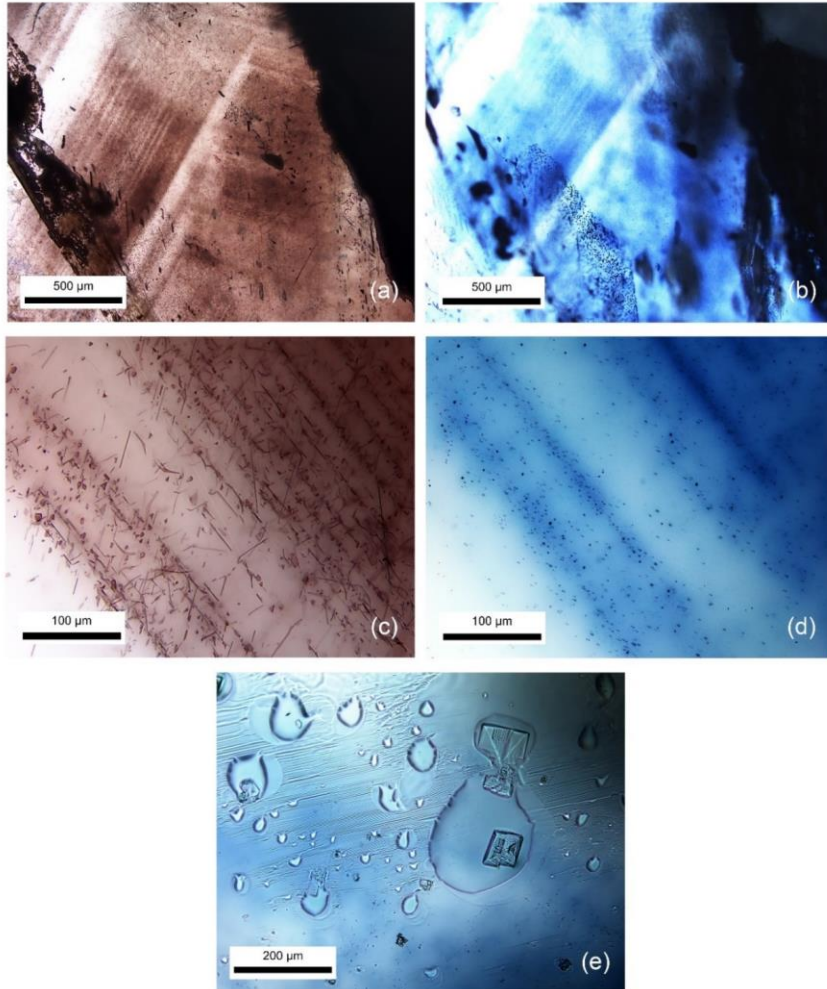
243 3.3 Microscopic features

244 Negative crystals, with or without CO₂ gas bubbles, were commonly observed alongside mineral inclusions,
245 such as oligoclase feldspar, calcite, and muscovite, in these sapphire samples. Brown silk inclusions were
246 prominent in both HS and LS groups, as shown in Fig. 2 (G22SF, G18LS, and G04HS for Fig. 2a, Fig. 2b–
247 c, and Fig. 2d–f, respectively). Micro-Raman spectroscopy was used to identify CO₂ and mineral
248 inclusions. Although brown silk inclusions, typically needle-shaped and aligned with color banding (Fig.
249 3a), were often less than 1 μm in diameter and difficult to identify, irregular or flaky platelet forms (Fig.
250 3c) were also noted. Negative crystals with/without CO₂ gas bubble appeared to be the common internal
251 feature as well as mineral inclusions (e.g., oligoclase feldspar, calcite, and muscovite) that were usually
252 found in these sapphire samples. Additionally, brown silk inclusions were clearly recognized in high-
253 density silk and low density silk groups. Fig. 2 presents the most common micro inclusions found in these
254 samples. Micro Raman spectroscopy was applied for identification of CO₂ and mineral inclusions.
255 However, brown silk inclusions, usually oriented along the color banding/zoning (Fig. 3a), were very tiny
256 (less than 1 μm in diameter) and rather difficult to be identified by any technique. These silk inclusions
257 were typically needle-shaped, however, thin, irregular, or flaky platelets of silk inclusions (Fig. 3c) also
258 appeared in these sapphire samples.
259 3c) were also noted.



260
 261 **Figure 2.** Photomicrographs of inclusions including CO₂-containing
 262 negative crystals (a), calcite (b), cluster of negative crystals (c), oligoclase (d), muscovite (e), and brown
 263 silks (f) in natural unheated sapphire.
 264

265 After high-temperature heating, molten surfaces (Fig. 3e) and decomposed crystal
 266 inclusions were commonly observed in these sapphire-samples. The most notable alteration was also
 267 detected in the initial area of brown silks (Fig. 3a), which exhibited distinct bluish color banding/zoning
 268 (Fig. 3b) after heating.
 269

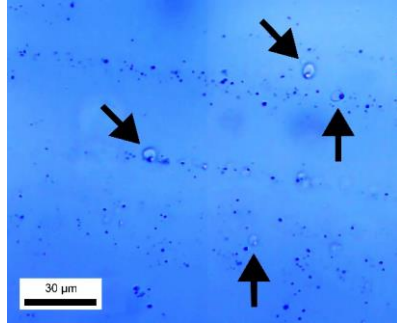


270
 271 **Figure 3.** Transmitted-light photomicrographs showing that brown banding (a) with irregular platy
 272 brownish flakes and tiny needles (c) in natural unheated sapphire samples turned into
 273 blue color banding (b) with blue dots (d) after heating. Melted surface (e) was also observed after
 274 heat treatment.

275

276 The brown silks (Fig. 3c) experienced a transformation upon heating into blue dots (Fig.
 277 3d). Additionally, melt inclusions among blue dots were likely developed by melting of brown silks with
 278 collaborative reaction of the sapphire host, which have never been reported elsewhere, becoming
 279 significantly noticeable and useful for indicating heat treatment of sapphire (Fig. 4).

280



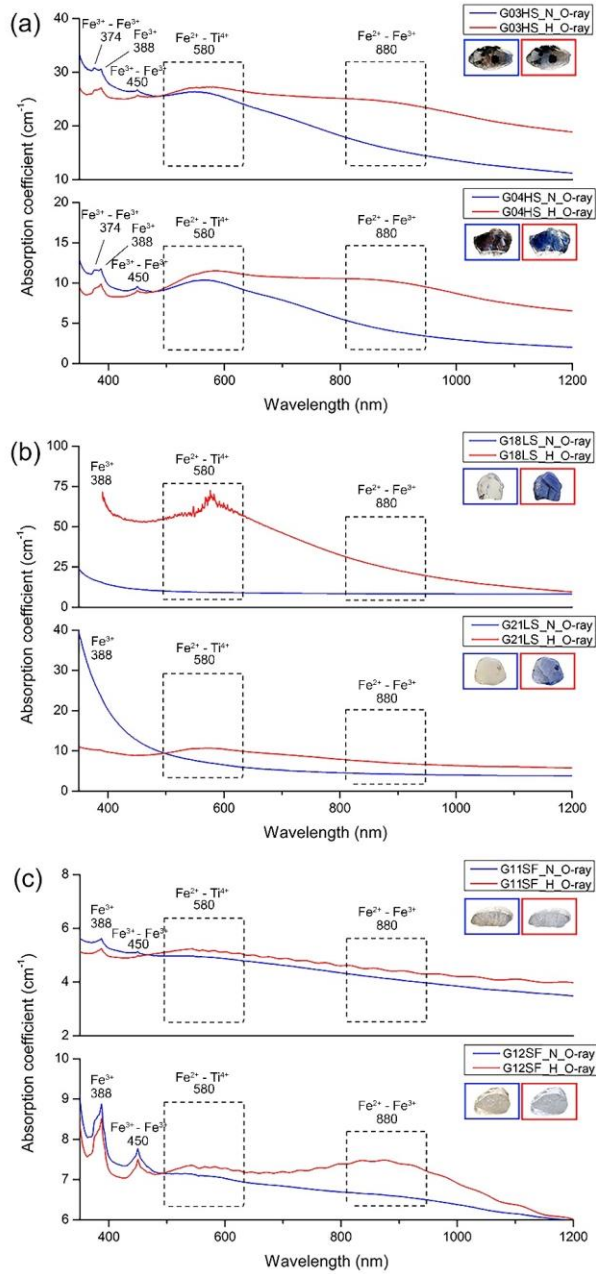
281

282 **Figure 4.** Transmitted-light photomicrograph showing melt inclusions (arrows) among blue dots
283 transformed from silk inclusions in sapphire after heating (sample G04HS).

284

285 3.4 Optical (UV-VIS-NIR) spectroscopy

286 The optical spectra of representative sapphire samples are presented in Fig. 5. Absorption peaks at 374,
287 388, and 450 nm, as well as bands around 580 and 880 nm, were observed. Optical spectra have been
288 studied on unheated and heated sapphire by numerous previous researchers (e.g., Ediriweera and Perera,
289 1989; Perera et al., 1991; Emmett and Douthit, 1993; Hughes, 1997; Kyi et al., 1999; Emmett et al., 2003;
290 Sriponjan et al., 2014; Hughes, 2017; Pisutha-Arnond, 2017; Themelis, 2018; Palke et al., 2019;
291 Soonthorntantikul et al., 2019; Dubinsky et al., 2020). The 374, 388, and 450 nm peaks as well as the 880
292 nm band were proposed to be attributed to Fe, the 580 nm band to the Fe-Ti pair. After heating, all samples
293 showed a significant increase in the main Fe-Ti pair related absorption band at around 580 nm (Figs. 5a-
294 c), whereas Fe-Fe related absorption at around 880 nm was obviously increased in some samples (i.e.,
295 Figs. 5a and 5c). The intensified absorption of the 580 nm band in these samples is referred to an increase
296 of Fe-Ti pairs after heating which leads to enhanced blue coloration in heated sapphires.



297

298 **Figure 5.** Optical absorption spectra of untreated (blue lines) and heated (red lines) samples: (a) **high-**299 **density-silkHS** group (G03HS, G04HS); (b) LS group (G18LS, G21LS); (c) **silk-freeSF** group (G11SF,

300 G12SF). Sizes of stones range between 0.4 and 12 mm.

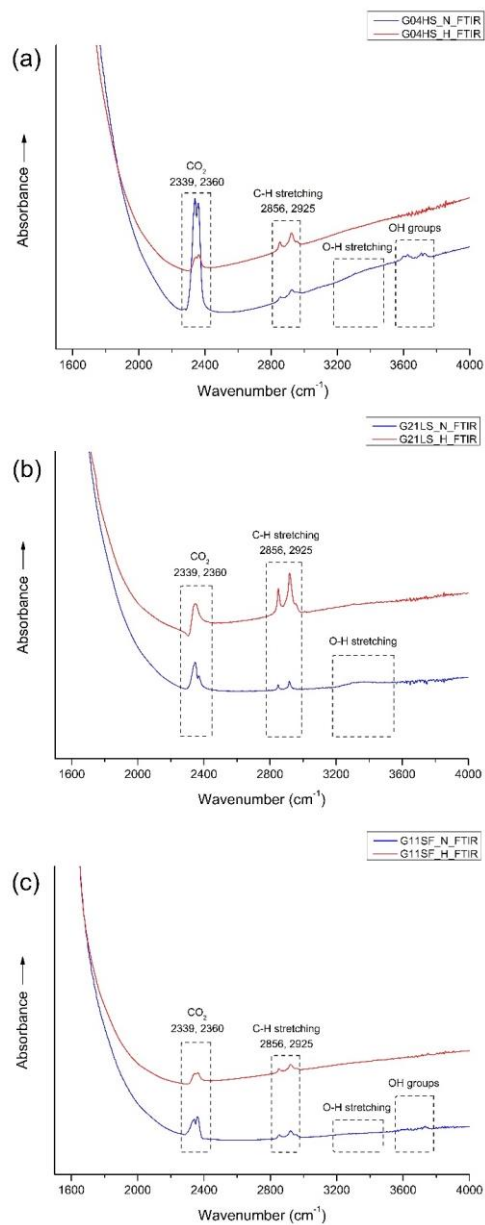
301

302 Spectral characteristics of corundum containing Fe^{3+} ions exhibit a high degree of
 303 complexity. It is noteworthy that Fe^{3+} has electron configuration d^5 resulting in a crystal field spectrum
 304 with ground state ${}^6\text{A}_1$ (Ferguson and Fielding, 1972). Small peaks at 374 nm (${}^4\text{E}^b$) and 450 nm (${}^4\text{A}_1, {}^4\text{E}^a$)
 305 should be attributed to the enhanced absorption of Fe^{3+} – Fe^{3+} pairs (McClure, 1962; Ferguson and Fielding,
 306 1971; Krebs and Maisch, 1971; Ferguson and Fielding, 1972) as well as a weak broadband absorption at
 307 540 nm (${}^4\text{T}_2$) which could not be seen in this work. The distinct peak observed at a wavelength of 388 nm
 308 (${}^4\text{T}_2^b$) (Krebs and Maisch, 1971) is linked to the individual Fe^{3+} ions. This, however, does not rule out the
 309 possibility of a higher-order cluster with extra ions or other point defects (Emmett et al., 2003).
 310 Additionally, there is also a broad band at a wavelength of 330 nm (${}^4\text{T}_1^b$) which is interpreted as a Fe^{3+} –
 311 Fe^{3+} pair absorption (Ferguson and Fielding, 1972). This is also present in the spectra of heated samples
 312 G03HS and G04HS, as well as in all spectra of sample G12SF in this study. In trace contents both Fe^{2+} (d^6)
 313 and Ti^{4+} (d^0) ions alone do not exhibit any absorption in corundum in the visible range (Townsend, 1968);
 314 on the other hand, Fe^{2+} – Ti^{4+} pairs ($t_2 \rightarrow {}^2\text{E}$) (Ferguson and Fielding, 1971) may yield a broad band
 315 absorption around 580 nm (E||c), or 700 nm (E||c) (Dubinsky et al., 2020). The Fe^{2+} – Fe^{3+} pair gives rise
 316 to the broad absorption band at ca. 880 nm (Fig. 5; Ferguson and Fielding, 1972).

317

318 3.5 FTIR spectroscopy

319 FTIR spectra of most samples yielded identical patterns within the range of 1600–4000 cm^{-1} (Fig. 6).
 320 They usually showed CO_2 peaks (at 2339 and 2360 cm^{-1}), as well as C–H stretching related peaks (at
 321 2856 and 2925 cm^{-1}), likely from artefacts turbidity (Fig. 6, blue lines), in accordance with Hughes
 322 (2017) (2017) and Soonthorntantikul et al. (2021). However, O–H stretching of boehmite/diaspore peaks
 323 (at 1975 and 2105 cm^{-1}) (Delattre et al., 2012; Sun et al., 2015; Choi et al., 2017; Filatova et al., 2021;
 324 Soonthorntantikul et al., 2021) was only observed in sample G03HS from the high-density-silk group (Fig.
 325 7a, blue line). Weak absorption features of O–H stretching from H_2O (broad band at ca. 3400 cm^{-1}) and
 326 OH groups (ca. 3600–3700 cm^{-1}) were only found in the untreated samples (blue lines), see Fig. 6a.



328

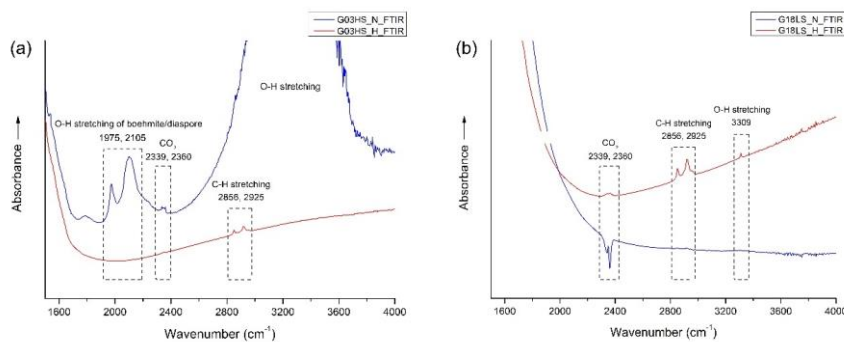
329 **Figure 6.** FTIR spectra obtained before (blue lines) and after (red lines) heating experiments of

330 representative samples G04HS (a), G21LS (b), and G11SF (c) of the high-density-silk group (a), low-

331 density-silk group (b), and silk-free group (c), respectively.

332

333 After heating, boehmite/diaspore-related absorption peaks (only observed in sample
 334 G03HS of the high-density silk group, Fig. 7a) at 1975 and 2105 cm^{-1} disappeared. In contrast, the 3309
 335 cm^{-1} hydroxyl (O-H) absorption, which was not present in any natural sample before heating, appeared
 336 only in sample G18LS of the low-density silk group after heating (Fig. 7b, red line). It should also be
 337 mentioned that the presence of CO_2 peaks at 2339 and 2360 cm^{-1} , as well as the C-H stretching related
 338 peaks at 2856 and 2925 cm^{-1} of all samples remained the same after heating. In contrast, their intensities
 339 vary dramatically (see Figs. 6 and 7).
 340



341
 342 **Figure 7.** FTIR spectra obtained before (blue lines) and after (red lines) heat treatment of samples G03HS
 343 of high-density silk group (a) and G18LS of low-density silk group (b).
 344

345 To detect the heat treatment in corundum, FTIR spectroscopy is a recommended tool. In
 346 some circumstances, the presence or absence of certain FTIR features in the O-H absorption region (3100–
 347 3600 cm^{-1}) could be used as an indicator of heat treatment (Smith, 1995; Beran and Rossman, 2006;
 348 Saeseaw et al., 2018; Saeseaw et al., 2020). For example, the presence of the 3309 cm^{-1} FTIR absorption
 349 peak was used as an indicator of heated corundum (Hughes and Perkins, 2019; Saeseaw et al., 2020;
 350 Soonthorntantikul et al., 2021). However, there were some inconsistencies presented recently: in some
 351 cases the 3309 cm^{-1} peak was also found in unheated sapphire, thus it is not a reliable indicator of heat
 352 treatment (Hughes, 1997, 2017; Hughes and Perkins, 2019; Saeseaw et al., 2020; Soonthorntantikul et al.,
 353 2021).

354 In this study, an absence of O-H absorption in the 3100–3600 cm^{-1} range in all natural
 355 geuda sapphire samples, together with the development of a weak absorption at 3309 cm^{-1} upon heating in
 356 only one of the samples (see Fig. 7b, red line), address the limitation to differentiate unheated and heated
 357 sapphire by FTIR spectroscopy. Furthermore, heat treatment employed in this study did not involve the use
 358 of any additional gases, such as hydrogen, to create a reducing atmosphere within the furnace. Despite this,
 359 the 3309 cm^{-1} absorption band was seen after the heating process. This might be in accordance with an
 360 explanation proposed earlier by Notari et al. (2018).

361 The controversy of the presence of an O-H peak in the FTIR spectrum in unheated and
 362 heated sapphire could be attributed to an inherent hydrogen content of the corundum. Hydrogen was found
 363 in corundum, primarily in the form of alumina hydrates (Notari et al., 2018). These hydrates could release

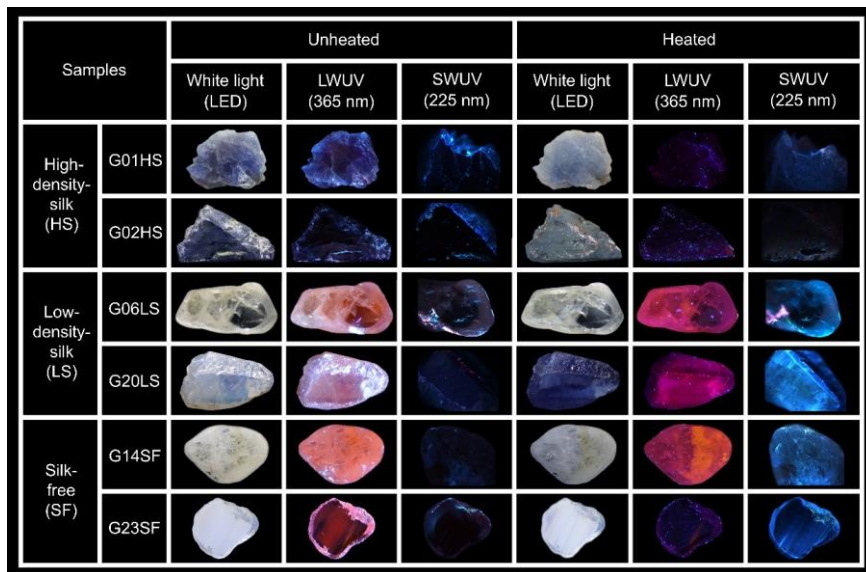
364 hydrogen through de-hydroxylation at temperatures as low as approximately 450 °C.
 365 Additionally, hydrogen was present in the air as H₂O, which can be split at temperatures around 900 °C to
 366 produce hydrogen gas (H₂) and oxygen gas (O₂) through the reaction $2\text{H}_2\text{O} \rightarrow 2\text{H}_2 + \text{O}_2$ (Notari et al.,
 367 2018).

368

369 3.6 Photoluminescence imaging and spectroscopy

370 Photos presenting luminescence of some samples both before and after heat treatment are
 371 shown in Fig. 8. Before heating, all natural sapphire samples were inert to SWUV light; moreover, all low-
 372 density-silkLS and silk-freeSF samples exhibited orange to red luminescence under LWUV light (Fig. 8).
 373 After heating, all low-density-silkLS and silk-freeSF samples, exhibited intense blue luminescence under
 374 SWUV light whereas their initial orange to red luminescence under LWUV light turned into a strong
 375 purplish red luminescence (Fig. 8, samples G06LS and G20LS in particular). In summary, the high-density-
 376 silkHS samples were all inert to SWUV and LWUV light both before and after heating. Notably under
 377 LWUV light, an initial orange to red luminescence of a few samples from the silk-freeSF group was
 378 drastically reduced after heating (e.g., G23SF in Fig.8).

379



380

381 **Figure 8.** Representative images of high-density-silkHS (G01HS, G02HS), low-density-
 382 silkLS (G06LS, G20LS), and silk-freeSF (G14SF, G23SF) groups obtained under LWUV and SWUV
 383 illumination before and after heating. Sizes of stones range between 4 mm and 12 mm.

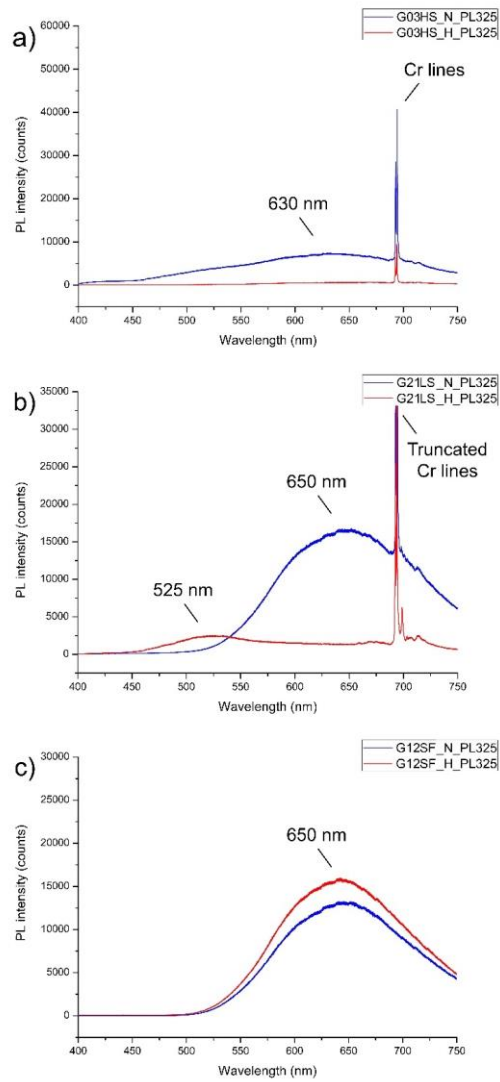
384

385 The UV-excited photoluminescence-PL (PL) spectra showed that all the unheated
 386 and heated sapphire samples have an identical feature of two narrow peaks of trace Cr³⁺ lines at around
 387 692.8 and 694.2 nm (Fig. 9) that are assigned to the spin-forbidden ²E → ⁴A₂ relaxation of trace Cr³⁺
 388 (Nelson and Sturge, 1965). However, the Cr³⁺ lines of some samples (Fig. 9c) are too weak to be visible

389 within the noise of a broad and strong emission band. All unheated sapphire samples showed a similar
390 emission band in the orange to red region centered around 630–650 nm (Fig. 9a–c, blue line). Remarkably,
391 this appears to be associated with orange to red luminescence under LWUV light, as noted by (Segura,
392 2013; Vigier et al., 2021a, b, c; Vigier and Fritsch, 2022). Despite having the emission band around 630–
393 650 nm, only unheated sapphire ~~from HS group s with high density silk~~ appeared inert under LWUV
394 illumination while the others revealed orange to red luminescence.

395 After heating, significant alteration in the emission band was observed, as depicted by
396 the red lines in Fig. 9a–c. The photoluminescence spectra of sample G03~~HS from the high density silk~~
397 ~~group~~ exhibited a notable reduction in the emission band through the visible region (Fig. 9a, red line). This
398 went along with a lack of luminescence both under SWUV and LWUV excitation, whereas sample G12~~SF~~
399 ~~(silk free group)~~ demonstrated a slight increase of the emission band in the orange to red region (Fig. 9c,
400 red line). More details are given in the discussion part below.

401 In contrast to the other groups, after heating, sample G21~~LS of the low density silk~~
402 ~~group~~ (Fig. 9b, red line) exhibited a significant emission band in the green region at around 525 nm. Note
403 that this broad emission is excited with the 325 nm laser (Fig. 9) but does not seem to affect significantly
404 the emission colors observed under SWUV (254~~225~~54 nm) and LWUV (365 nm) excitation (Fig. 8). For
405 a discussion of the possibly strong dependence of emission intensity (and color) on the excitation
406 wavelength see for instance Zeug et al. (2022). Likewise heated sapphire has been proposed to have an
407 emission band in the blue region, which corresponds to blue luminescence under SWUV light (Nassau,
408 1981; Hughes, 2017; Vigier et al., 2023).



410
 411 **Figure 9.** Representative photoluminescence (UV-excited) spectra obtained before (blue lines) and after
 412 (red lines) heating of sample G03HS of high-density-silk-group (a), sample G21 of low-density-silk
 413 group G21LS (b), and sample G12 of silk-free group G12SF (c).

414

415 4 Discussion

416

417 4.1 Generalities

418 After Ti⁴⁺ being exposed to SWUV light, they yield luminescence (Nasdala and Fritsch,
 419 2024). However, blue luminescence was not observed in both unheated and heated basaltic sapphire,
 420 possibly due to the abundant presence of Fe²⁺ of basaltic origin that may strongly quench such blue
 421 luminescence (Soonthorntantikul et al., 2019). More details will be discussed in this report. Furthermore,
 422 even though microscopic inclusions have been the distinguishing characteristics of heated sapphire,
 423 identifying heat-treated sapphire remains challenging (Crowningshield, 1966; Hughes, 2017). FTIR
 424 spectroscopy havehas- also been applied to detect heated sapphire. In some cases, the presence or absence
 425 of specific FTIR features in the O–H absorption region (3100–3600 cm⁻¹) may serve as an indicator of heat
 426 treatment (Smith, 1995; Beran and Rossman, 2006; Saeseaw et al., 2018); however, it is probably not a
 427 conclusive evidence (Ediriweera and Perera, 1989; Perera, 1993; Sutthirat et al., 2006; Cartier, 2009; Jaliya
 428 et al., 2020). For example, the presence of the 3309 cm⁻¹ FTIR absorption peak was used as an indicator of
 429 heated corundum (Hughes and Perkins, 2019; Soonthorntantikul et al., 2021). However, recent discoveries
 430 show that this peak may also be found in unheated sapphire, suggesting that it is not a reliable indication
 431 of heat treatment indication (Hughes, 1997, 2017; Hughes and Perkins, 2019; Soonthorntantikul et al.,
 432 2021).

Commented [TP1]: Moved from introduction to discussion

Commented [TP2R1]: Moved from lines 99-109 to here as suggested by R#2

Commented [TP3]: Moved from result part to discussion part

Commented [TP4R3]: Moved from lines 349-354 to here and revised as suggested by R#2

4.2.1 Silk inclusions and coloration of sapphire

435 Studies addressing brown silk inclusions in corundum are scarce. Soonthorntantikul et al. (2021) reported
 436 a mix of whitish silk and irregular/flaky/platelet-like brownish silk inclusions in corundum from Mogok.
 437 Brown silk was ascribed as presumable ilmenite (FeTiO₃) which is noticeable in high-Fe sapphire,
 438 whereas white silk was suggested to consist of rutile (TiO₂). The brown silks seen in our sapphire samples
 439 are likely ilmenite, which is supported by their irregular/flaky/platelet-like brownish appearance and their
 440 high Fe and Ti contents (note that the highest quantity of Fe was found in the HS group). Ilmenite
 441 decomposition upon heat treatment does result in Fe and Ti migration into the host sapphire and
 442 subsequently causes blue coloration. In particular, the decomposition of brown silks during heat treatment
 443 induces the formation of blue dots, which is a result of the Fe²⁺–Ti⁴⁺ pairing formation. Upon closer
 444 inspection using a high-resolution microscope, these blue dots reveal distinct micro-inclusions as melt
 445 inclusions (with size of ≤1 μm, see Fig. 4), which have never been documented before. However, it should
 446 be noted that these melt inclusions are possibly derived from the decomposition of silks.

447 This work focuses only on blue coloration in sapphire which mainly relates to the Fe²⁺–
 448 Ti⁴⁺ pair, as initially noted by Townsend (1968), followed by Mattson and Rossman (1988), Moon and
 449 Phillips (1994), and Emmett et al. (2003). Ti exhibits electron-donor properties, whereas Fe may function
 450 as an electron acceptor. When occupying neighboring Al³⁺ positions, absorption due to intervalence charge
 451 transfer between such donor-acceptor pairs may occur (details reported by Emmett et al., 2003 and
 452 Monarumit et al., 2023).

453 It should also be mentioned that Ti⁴⁺ ions do not exhibit any absorption characteristics in
 454 the visible spectrum when considered individually. The Ti⁴⁺ ion has a closed-shell electron configuration,
 455 whereas the Fe²⁺ ion mainly absorbs wavelengths within the near infrared and low-energy visible regions.
 456 In contrast, when Fe²⁺ and Ti⁴⁺ ions are situated on neighboring structural sites, notable absorption bands

457 develop across the visible and near-infrared spectral regions. These Fe^{2+} - Ti^{4+} pairs exhibit a band center
 458 at around 580 nm (see Fig. 5) when the electric field vector E is perpendicular to the crystallographic c -
 459 axis ($E \perp c$), but a peak at 700 nm is seen when the electric field vector E is parallel to the crystallographic
 460 c -axis ($E \parallel c$) (Dubinsky et al., 2020). Although the theory of the energy levels of an individual transition
 461 metal ion inside a crystal has been extensively explored, the corresponding theory for ion pairs or clusters
 462 within a crystal remains underdeveloped (Dubinsky et al., 2020).

463 In ~~this~~ the present study, the natural unheated geuda sapphire samples were placed in
 464 atmospheric conditions and subjected to a maximum temperature of 1650 °C for a duration of 10 h.
 465 According to the ~~ex~~ samples presented in Fig. 1, samples G03~~HS~~ and G04~~HS~~ ~~with high-density silk~~
 466 ~~inclusions~~ exhibited a noticeable increase in blue coloration, particularly around the area of brown silks
 467 and brown color banding/zoning, after heating. On the other hand, the initial blue patch (e.g. samples
 468 G01~~HS~~ and G02~~HS~~) became paler blue after heating, which might be due to the breakage of initial Fe - Ti
 469 pairs in those areas. The other groups, which have yellowish and/or milky appearances, revealed an increase
 470 in blue color after heating (samples G12~~SF~~ and G18~~LS~~, Fig. 1). This blue coloration is attributed to two
 471 distinct factors, notably the ~~dissolving~~ decomposition of silk inclusions and a subsequent charge transfer
 472 mechanism (Emmett and Douthit, 1993; Hughes, 1997, 2017; Nassau, 1980, 1981; Themelis, 2018). The
 473 process of charge transfer (Ferguson and Fielding, 1972; Nassau, 1981) is described as:



475 It is important to note that the blue color observed in sapphire could also be produced
 476 with the application of heat in oxidizing conditions at high temperature. Heat treatment can be classified as
 477 high- or low-temperature according to the decomposition of rutile silks in corundum (Nassau, 1981;
 478 Emmett and Douthit, 1993; Emmett et al., 2003; Hughes, 2017; Hughes and Perkins, 2019). The term low-
 479 temperature heat treatment has been used (typically referred to as below 1000 °C) when rutile particles still
 480 reveal their original structures. On the other hand, temperatures beyond 1350 °C denote high-temperature
 481 heat treatment when rutile silks start to decompose and dissolve within the corundum host (Hughes, 2017;
 482 Themelis, 2018). Consequently, internal diffusion (indicated by a colored halo surrounding the crystal
 483 inclusion), molten or altered inclusions, and/or broken silk are strong indicators of high-temperature heat
 484 treatment. However, low-temperature heat treatment can also produce various altered mineral inclusions
 485 (Kammerling et al., 1990; McClure and Smith, 2000; McClure et al., 2010; Pisutha-Armond, 2017;
 486 Soonthorantikul et al., 2019).

487 In recent studies, the possibility of employing Fe^{2+} - Fe^{3+} charge transfer as an alternate
 488 method for blue coloration has also been mentioned (Nikolskaya et al., 1978; Schmetzer and Kiefert, 1990;
 489 Häger, 1992, 2001; Sripoonjan et al., 2014; Pisutha-Armond, 2017). However, it is necessary to emphasize
 490 that this approach was considered highly improbable (Nassau, 1981). Nevertheless, previous studies have
 491 indicated that a minor proportion of geuda sapphire from Sri Lanka and geuda-like sapphire from Mogok
 492 in Burma revealed an alteration in color to blue when subjected to heating in an oxidizing environment
 493 (Hughes, 1997, 2017; Kyi et al., 1999), which is in complete contradiction to the treatment method
 494 employed for the geuda sapphire in a reducing condition. The appearance of certain stones displaying a
 495 blue coloration under oxidizing conditions might be attributed to the presence of ilmenite silks, which is
 496 composed of Fe and Ti, with Fe in its reduced Fe^{2+} state (Hughes, 1997). Therefore, it is unnecessary to

Commented [TP5]: Moved from introduction to discussion

Commented [TP6R5]: Moved from lines 78-87 to here as suggested by R#2

497 reduce Fe^{3+} to Fe^{2+} ions to generate the $\text{Fe}^{2+}\text{-Ti}^{4+}$ pairs that are responsible for the manifestation of the
 498 blue color. Hence, the blue areas have a substantial concentration of Fe ions in form of Fe-Ti pairs, derived
 499 from the decomposed ilmenite silk inclusions.

500 According to Nassau (1981) and Koivula (1987), the presence of blue dots in heated
 501 sapphire is attributed to remains of dissolved silk inclusions and internal cation diffusion. The diffusion
 502 process is positively correlated with temperature and duration of heat treatment (Nassau, 1981). Despite
 503 the slow diffusion rates of Fe and Ti, the distances across are extremely short, i.e., just a few micrometers
 504 (Nassau, 1981). Consequently, a potential Fe-Ti combination within the corundum's lattice may generate
 505 the blue dots.

506 The presence of melt inclusions among the blue dots after high-temperature heating
 507 might be due to the decomposition of brown silk and its solubility into the host sapphire as demonstrated
 508 by Jung et al. (2009). They predicted a phase relationship within the $\text{Al}_2\text{O}_3\text{-Ti}_2\text{O}_3\text{-TiO}_2$ system based on
 509 experimental data and thermodynamic calculation. Consequently, they suggested that a liquid phase (the
 510 composition of the liquid inclusion phase varies significantly between Al_2O_3 and Ti_3O_5) could possibly be
 511 present at a temperature of 1600 °C and slightly below, which is close to the heating temperature (1650 °C)
 512 of our experiment. Silk inclusions as represented by $\text{Ti}_2\text{O}_3\text{-TiO}_2$ components may have dissolved into the
 513 host sapphire (Al_2O_3 component), and produced a proper composition of solution which could be melted
 514 partially at ≤ 1650 °C. Some of these melts can be preserved as inclusions after cooling down.
 515

516 **4.3.2 Luminescence of sapphire**

517 Luminescence of corundum may be assigned to two types, namely (a) emissions of
 518 impurity-related centers such as Ti^{4+} (commonly known) and (b) emissions of defect-related centers,
 519 which typically involve either vacancies, such as oxygen (O) or aluminum (Al) vacancies known as F
 520 center (color center; from the German "*Farbzentrum*"), or interstitials (Al_i and O_i), possibly trapped at
 521 impurities (less known), or both (Viger et al., 2021a-c). This means that defect-related emission centers
 522 in corundum refer to an inconsistency in the atomic arrangement limited to one or a few atoms (often called
 523 color-centers). O vacancies (or electron holes) are sometimes called hole centers, because the holes simply
 524 designate the absence of an electron. The holes are sometimes filled with one or two electrons in order to
 525 maintain electroneutrality (Vigier et al., 2021a).

526 As presented in Fig. 8, a notable orange to red luminescence is easily noticeable under
 527 LWUV excitation in most unheated sapphire samples, except for those of the [high-density-silkHS](#) group,
 528 which appear inert. After heat treatment, the orange to red luminescence that is initially observed in all
 529 samples of the [low-density-silkLS](#) group and many samples of the [silk-freeSF](#) group turns into a purplish-
 530 red luminescence. In contrast, no orange to red or purplish red luminescence is observed in any sample of
 531 the [high-density-silkHS](#) group both before and after heating.

532 The origin of orange to red luminescence in sapphire remained controversial, with
 533 varying ideas among researchers (Vigier et al., 2021a, b, 2023). The occurrence of orange luminescence
 534 has been documented in some previous studies (e.g. Spencer, 1927; Kane, 1982; Emmett et al., 2003;
 535 Fritsch et al., 2003; [Nasdala and Fritsch, 2024](#)). In the beginning, it was hypothesized that this luminescence
 536 is associated with the geographic origin of yellow sapphire from Sri Lanka (Webster, 1984). Subsequently,

537 Segura (2013)(2013) presented an alternative argument to this notion, suggesting the presence of orange
538 luminescence in various colors of corundum, regardless of treatment or synthetic origin, might be attributed
539 to the existence of some defects. However, the orange to red luminescence observed in our study
540 (characterized by a broad emission band) seems to be associated with complex defect-related centers. ~~As~~
541 ~~previously stated, orange to red luminescence was proposed to be attributed with an F-center or defect~~
542 ~~characterized by the occurrence of two O vacancies (Vigier et al., 2021a, b). An O vacancy refers to the~~
543 ~~absence of an O atom in the structure. It has the potential to remain an empty vacancy or to incorporate one~~
544 ~~or two unpaired electrons (Vigier et al., 2021a, b).~~

545 However, it is possible that these defects may originate from boehmite/diaspore, which
546 undergo oxidation (Strange et al., 2022), dehydration (Gog, 2021), or dehydroxylation (Ananthakumar et
547 al., 1998) at temperatures exceeding 400 °C (Vlaskin et al., 2016). This process occurs through the
548 decomposition of $2\text{AlO}(\text{OH}) \rightarrow \text{Al}_2\text{O}_3 + \text{H}_2\text{O}$ (Klopprogge et al., 2002; Sifontes et al., 2019). Therefore,
549 when subjected to heating, these hydrated aluminas decompose and expell water (Samadhi et al., 2011).
550 This could result in the development of defects related to dehydration (Gog, 2021), which may be linked to
551 the F-center as mentioned above.

552 Orange to red luminescence in sapphire is not due to impurities (Vigier et al., 2021a, b).
553 HS sapphire (e.g., with ilmenite, FeTiO_3) lack noticeable luminescence, likely because Fe^{2+} suppresses
554 luminescence, contrasting with LS and SF sapphire, which display stronger luminescence both before and
555 after heating. While sample G23SF shows decreased purplish-red luminescence after heating, most display
556 increased purplish-red luminescence, potentially due to complex, defect-related centers in the sapphire
557 lattice. Observations suggested that Fe^{2+} acts as a luminescence quencher in the orange to red range
558 (Andrade et al., 2008; Norrbo et al., 2016; Vigier et al., 2021a, b, c; Vigier and Fritsch, 2022); Orange
559 luminescence generally appears in colorless, low-Fe areas (Segura, 2013; Notari et al., 2003). However, a
560 definitive explanation remains unresolved. Furthermore, it is important to note that the orange to
561 red luminescence is not attributed to any impurities (Vigier et al., 2021a, b). In addition, the absence of
562 noticeable luminescence in high density silk sapphire samples (see Fig. 8), both before and after heat
563 treatment, can be attributed to the presence of significant amounts of brown silks (ilmenite, FeTiO_3), where
564 Fe^{2+} is suggested to play an important role to suppress luminescence. This contrasts with samples of the
565 low density silk and silk free groups, which exhibit more distinct orange to red luminescence both before
566 and after heating. Even though an orange to red luminescence of a few samples (e.g., G23) decreases after
567 heating, increasing of orange to red luminescence to a purplish red luminescence in most samples upon
568 heating is generally observed (Fig. 8). This might be due to the remaining of altered, complex defect related
569 centers in the sapphire lattice as mentioned earlier whereas the disappearance of orange to red luminescence
570 in a few samples (see Fig. 8, sample G23) might be due to the disappearance of defects after heating.
571 Moreover, the orange luminescence was proposed to be seen generally in colorless areas (Segura, 2013),
572 which were described later on as low Fe containing areas (Notari et al., 2003). Therefore, Fe^{2+} serves as a
573 quencher of luminescence for emissions in the orange and red spectral range (Andrade et al., 2008; Norrbo
574 et al., 2016; Vigier et al., 2021a, b, c, 2023; Vigier and Fritsch, 2022). However, an exact clarification has
575 never been established.

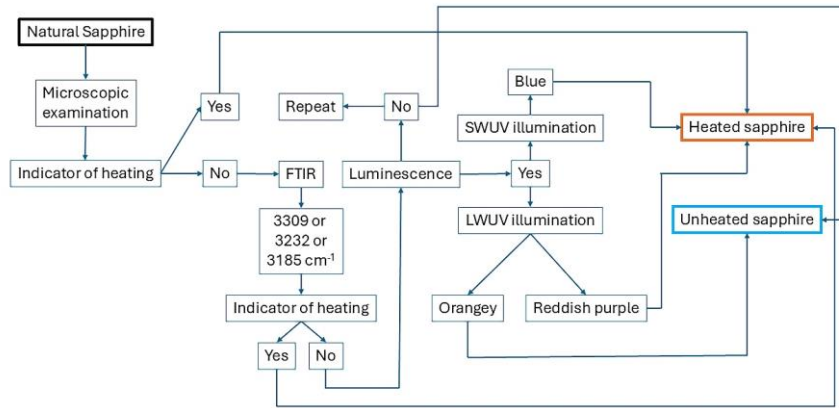
Regarding blue luminescence, it has been observed that upon exposure to SWUV light, all natural unheated sapphire samples appeared inert. After heating, apart from high-density-silk HS sapphire, a distinct blue luminescence has been detected throughout most heated sapphire samples (Fig. 8). Previous studies suggest that luminescence in sapphire becomes noticeable only at heating temperatures of 1000 °C. It was previously suggested that luminescence in sapphire is not noticed until they are heated up to a temperature of 1000 °C (Hughes and Perkins, 2019), at which point blue luminescence is linked to heat treatment detection. This luminescence is believed to arise from silk inclusions composed of TiO₂, commonly found in natural blue sapphire. At this point, the discernible blue luminescence observed in sapphire has been linked to the detection of heat treatment. This blue luminescence was proposed to be attributed to the presence of silk (Hughes and Perkins, 2019) since the majority of natural blue sapphire usually show the exsolved silk, which is composed of TiO₂. Notably, despite the relatively low Ti concentration (0.02–0.03 wt% oxide) in comparison to Fe (0.05–0.08 wt% oxide) in some samples (e.g., G12SF and G21LS of the silk-free and low-density-silk groups, respectively), blue luminescence remains this blue luminescence is still detected. In contrast, HS samples (e.g., G02HS) show an absence of blue luminescence, likely due to the presence of ilmenite, supporting findings by Moreover, the absence of blue luminescence in high-density-silk samples (Fig. 8, sample G02) is likely attributed to the presence of ilmenite. This corresponds to previous studies conducted by Norrbo et al. (2016), Andrade et al. (2008), as well as Vigier et al. (2021a–c; 2023) that Fe²⁺ acts as a luminescence quencher. Blue luminescence has been associated with the interaction between O²⁻ and Ti⁴⁺ ions (Evans, 1994; Wong et al., 1995b; Nasdala and Fritsch, 2024), followed by a later hypothesis of a charge transfer process involving Ti⁴⁺ ions and certain defect-related centers (Lacovara et al., 1985; Mikhailik et al., 2005). However, it was widely accepted that the blue luminescence (characterized by a broad emission band at blue to green region) observed in sapphire under SWUV illumination is associated with the presence of Ti impurities, which are classified as element-related defects (Vigier et al., 2021a, b). Thus, it is likely that the blue luminescence reported in this work is associated with Ti impurities, whereas orange to red luminescence seems to be associated with complex defect-related emission centers.

The correlation between the orange to red PL emission band (approx. 650 nm, Fig. 9 blue lines) and orange to red luminescence in unheated sapphire (Fig. 8), as well as the emission band (approx. 525 nm, Fig. 9 red lines) and blue luminescence in heated sapphire (Fig. 8), is particularly evident in the LS group (Fig. 9b). In contrast, the HS group shows a reduction in emission across the visible spectrum after heating, indicating inertness under LWUV and SWUV excitation (Fig. 9a). The SF group exhibits a notable increase in the red emission band (Fig. 9c) and intense purplish-red luminescence under LWUV excitation after heating. Interestingly, this group also displays strong blue luminescence under SWUV excitation despite the absence of a corresponding blue emission band, likely due to the 325 nm excitation laser used in our PL investigation. Variations in excitation wavelengths significantly affect observed emissions, as noted by Wong et al. The correlation between the orange to red PL emission band (approx. 650 nm, Fig. 9 blue lines) and orange to red luminescence in unheated sapphire (Fig. 8), as well as the blue emission band (approximately 525 nm, Fig. 9, red lines) and blue luminescence in heated sapphire (Fig. 8), seem to correspond with each other only in samples from the low-density-silk group (Fig. 9b). The high-density-silk group exhibits a reduction in the emission band throughout the whole visible spectrum after

616 heating, corresponding to an inertness under LWUV and SWUV excitation (Fig. 9a). The significant
617 increase in the red emission band (Fig. 9c) of the silk-free group corresponds to an intense purplish-red
618 luminescence under LWUV excitation after heating. Notably it also displays a strong blue luminescence
619 under SWUV excitation after heating despite the lack of a blue emission band; this is possibly due to the
620 325 nm excitation laser used in our PL investigation. Due to absorption-emission conditions, it is obvious
621 that changing excitation wavelengths have substantial impact on the observed emission. Even in the narrow
622 range of 254, 325, or 365 nm UV excitation, significant differences in emission are expected. This was
623 presented by Wong et al. (1995a) and Vigier et al. (2023), who showed that their sapphire emission band at
624 425 nm was only visible with a 254 nm excitation laser. Utilizing distinct SWUV (225–54 nm) and LWUV
625 (365 nm) lasers, or conducting excitation spectroscopy, may yield more accurate results compared to
626 relying solely on a 325 nm laser. Thus, the presence of orange to red luminescence at approx. 650 nm and
627 blue luminescence at around 525 nm are vital indicators for differentiating unheated and heated sapphire,
628 whose sapphire emission band at 425 nm was obviously seen only with a 254 nm excitation laser. By
629 employing distinct SWUV (254 nm) and LWUV (365 nm) excitation lasers, or even by conducting
630 excitation spectroscopy, we may obtain more accurate results compared to using a 325 nm laser only.
631 Hence, the presence of orange to red luminescence and a broad emission band at approximately 650 nm,
632 along with blue luminescence and a broad emission band at around 525 nm, may serve as crucial indicators
633 for distinguishing unheated and heated sapphire.

635 5 Conclusions

636 The present study demonstrates that melt inclusions (~1 μm) serve as indicators of heat treatment
637 in sapphires and highlights the critical role of luminescence in distinguishing unheated from heated geuda
638 sapphire. Under LWUV light, orange luminescence may arise from defect-related F centers, while blue
639 luminescence under SWUV light likely correlates with Ti impurities. Geuda sapphires with low Fe
640 concentrations exhibit distinct luminescence, whereas those with HS inclusions show minimal
641 luminescence due to Fe²⁺ quenching effects. The presence of orange luminescence may be a helpful
642 indicator for unheated geuda sapphires, while blue luminescence is generally absent in unheated samples,
643 confirming its utility for identifying heated geuda sapphire. Although the 3309 cm⁻¹ O–H stretching band
644 from FTIR analysis alone is insufficient for differentiation, increased intensity around the 580 nm of an
645 optical spectra effectively indicates heat treatment, as it corresponds to higher Fe–Ti pair concentrations
646 from silk inclusion decomposition. Combining blue and/or purplish–red luminescence with additional
647 analytical techniques provides a promising strategy for accurately distinguishing between unheated and
648 heated geuda sapphires (Fig. 10). Future research should acquire emission and excitation spectra on the
649 samples before and after heat treatment. Further investigation of luminescence characteristics from various
650 sapphire origins (and colors) and clarify the specific Fe and Ti concentrations impacting luminescence is
651 also recommended. Finally, using as low as 200–254 nm laser excitation may enhance the detection of
652 emission shifts towards the blue region in heated sapphires, improving gemological identification criteria.



653

654 **Figure 10. Flowchart proposing a combined strategy for heated sapphire identification criteria.**

655 Overall, this work presents empirical evidence of the presence of melt inclusions ($\sim 1 \mu\text{m}$ in size) among
 656 blue dots serving as new hint of heat treatment. Additionally, the study highlights the significance of
 657 luminescence in distinguishing unheated sapphire from their heated counterparts.

658 Although the occurrence or disappearance of orange to red and blue luminescence has not been conclusively
 659 elucidated, the F-center (defect-related center) may be responsible for orange to red luminescence, whereas
 660 the blue one may be attributed to Ti impurities. Luminescence under SWUV and LWUV excitation is likely
 661 seen only in sapphire with low Fe concentration (as supported by chemical analysis), since we barely see
 662 luminescence in the group of high-density silk sapphire samples. However, the presence of orange to red
 663 luminescence under LWUV excitation may help in identifying unheated sapphire. Blue luminescence under
 664 SWUV light can also serve as a useful indicator for identifying heated sapphire since this luminescence,
 665 except for the high-density silk group, is absent in all unheated sapphires studied. This may be due to the
 666 interference-quenching effect of Fe^{2+} . In addition to blue, the presence of purplish-red luminescence under
 667 LWUV light may also facilitate the identification of heated sapphire. For the FTIR spectra, the 3309 cm^{-1}
 668 O-H stretching band alone seems to be insufficient to identify unheated or heated sapphire since the effect
 669 of additional gas used during the heat treatment as well as the internal diffusion may influence the
 670 appearance or absence of such an O-H feature. Also, an increase or elevated intensity of the optical spectra
 671 at an absorption around 580 nm may indicate heated sapphire, as the majority of heated sapphire samples
 672 exhibit a greater intensity in this band due to a higher number of Fe-Ti pairs, derived from a decomposition
 673 of silk inclusions after heating.

674 Thus, combining blue luminescence (and/or purplish-red luminescence) with additional analytical
 675 techniques represents a promising strategy for distinguishing unheated and heated sapphire. Further studies
 676 should be conducted to explore the luminescence properties of sapphire originating from different origins.
 677 This will contribute to a better understanding of the factors influencing the orange to red and blue
 678 luminescence observed in these sapphire samples. It is also essential to turn attention on comparing the
 679 luminescence characteristics shown by unheated and heated colored sapphire, as well as determining the

680 ~~precise Fe and Ti concentration required to affect orange to red and blue luminescence. Furthermore, to~~
681 ~~optimize the emission spectrum, it is recommended to utilize 254 nm laser excitation to obviously see a~~
682 ~~shift of the emission band towards the blue region of heated sapphire.~~

683

684 *Author Contributions.* T.P., C.S., B.W., L.N. conducted conceptualization, E.G.Z. acquired samples, T.P.,
685 C.S., B.W., L.N., C.C.N., M.W., E.L., G.G., T.S. conducted analyses and evaluation, T.P. wrote the
686 manuscript, all co-authors reviewed and edited the manuscript.

687

688 *Competing interests.* The ~~contact~~ corresponding author has declared that none of the authors has any
689 competing interests.

690

691 *Financial support.* This research is supported by the Second Century Fund (C2F) of Chulalongkorn
692 University (researcher number 80004543).

693

694 *Data Availability Statement.* Not applicable

695

696 *Acknowledgments.* This research is supported by the Second Century Fund (C2F) of Chulalongkorn
697 University (researcher number 80004543). We thank Andreas Wagner (Universität Wien) for sample
698 preparation and Sopit Poompeang (Chulalongkorn University, Bangkok) for assistance in EPMA analysis.
699 Finally, the first author acknowledges the use of QuillBot's artificial intelligence to facilitate grammatical
700 verification.

701

702 *Conflicts of Interest.* The authors declare that they have no conflict of interest.

703

704 6 References

705 Alombert-Goget, G., Li, H., Guyot, Y., Brenier, A., and Lebbou, K.: Luminescence and coloration of
706 undoped and Ti-doped sapphire crystals grown by Czochralski technique, *J. Lumin.*, 169, 516–
707 519, <https://doi.org/10.1016/j.jlumin.2015.02.001>, 2016a.

708 Alombert-Goget, G., Li, H., Faria, J., Labor, S., Guignier, D., and Lebbou, K.: Titanium distribution in
709 Ti-sapphire single crystals grown by Czochralski and Verneuil technique, *Opt. Mater.*, 51, 1–4,
710 <https://doi.org/10.1016/j.optmat.2015.11.016>, 2016b.

711 ~~Ananthakumar, S., Krishnapriya, G., Damodaran, A. D., and Warriar, K. G. K.: Thermal decomposition~~
712 ~~characteristics of boehmite gels under microwave heating and associated microstructural features,~~
713 ~~*Mater. Lett.*, 35, 95–99, [https://doi.org/10.1016/S0167-577X\(97\)00228-0](https://doi.org/10.1016/S0167-577X(97)00228-0), 1998.~~

714 Andrade, L. H. C., Lima, S. M., Novatski, A., Neto, A. M., Bento, A. C., Baesso, M. L., Gandra, F. C. G.,
715 Guyot, Y., and Boulon, G.: Spectroscopic assignments of Ti^{3+} and Ti^{4+} in titanium-doped OH-
716 free low silica calcium aluminosilicate glass and role of structural defects on the observed long
717 lifetime and high fluorescence of Ti^{3+} ions, *Phys. Rev. B*, 78, 224202,
718 <https://doi.org/10.1103/PhysRevB.78.224202>, 2008

- 719 Beran, A. and Rossman, G. R.: OH in naturally occurring corundum, *Eur. J. Mineral.*, 18, 441–447,
720 <https://doi.org/10.1127/0935-1221/2006/0018-0441>, 2006.
- 721 Cartier, L. E.: Ruby and sapphire from marosely, Madagascar, *J. Gemmol.*, 31, 171–180,
722 <http://doi.org/10.15506/JoG.2009.31.5.171>, 2009.
- 723 Choi, E., Song, K., An, S., Lee, K., Youn, M., Park, K., Jeong, S., and Kim, H.: Cu/ZnO/AlOOH catalyst
724 for methanol synthesis through CO₂ hydrogenation, *Korean J. Chem. Eng.*, 35, 73–81,
725 <https://doi.org/10.1007/s11814-017-0230-y>, 2018.
- 726 Crowningshield, R.: Developments and highlights at the gem trade lab in new york: Unusual items
727 encountered (sapphire with unusual fluorescence), *Gems Gemol.*, 12, 73, 1966.
- 728 Crowningshield, R.: Developments and highlights at GIA's lab in New York: Unusual fluorescence,
729 *Gems Gemol.*, 13, 120–122, 1970.
- 730 Delattre, S., Balan, E., Lazzeri, M., Blanchard, M., Guillaumet, M., Beyssac, O., Haussühl, E., Winkler,
731 B., Salje, E. K. H., and Calas, G.: Experimental and theoretical study of the vibrational properties
732 of diaspore (α -AlOOH), *Phys. Chem. Miner.*, 39, 93–102, <https://doi.org/10.1007/s00269-011-0464-x>, 2012.
- 733 0464–x, 2012.
- 734 Dubinsky, E. V., Stone-Sundberg, J., and Emmett, J. L.: A quantitative description of the causes of color
735 in corundum, *Gems Gemol.*, 56, 2–28, <https://doi.org/10.5741/gems.56.1.2>, 2020.
- 736 Ediriweera, R. and Perera, S.: Heat treatment of geuda stones – spectral investigation, *J. Gemmol.*, 21,
737 403–410, <https://doi.org/10.15506/jog.1989.21.7.403>, 1989.
- 738 Emmett, J. L. and Douthit, T. R.: Heat treating the sapphires of Rock Creek, Montana, *Gems Gemol.*, 29,
739 250–272, <https://doi.org/10.5741/gems.29.4.250>, 1993.
- 740 Emmett, J. L., Scarratt, K., McClure, S. F., Moses, T., Douthit, T. R., Hughes, R., Novak, S., Shigley, J.
741 E., Wang, W., Bordelon, O., and Kane, R. E.: Beryllium diffusion of ruby and sapphire, *Gems
742 Gemol.*, 39, 84–135, <https://doi.org/10.5741/gems.39.2.84>, 2003.
- 743 Evans, B. D.: Ubiquitous blue luminescence from undoped synthetic sapphire, *J. Lumin.*, 60–61, 620–
744 626, [https://doi.org/10.1016/0022-2313\(94\)90233-X](https://doi.org/10.1016/0022-2313(94)90233-X), 1994.
- 745 Ferguson, J. and Fielding, P. E.: The origins of the colors of yellow, green and blue sapphires, *Chem.
746 Phys. Lett.*, 10, 262–265, [https://doi.org/10.1016/0009-2614\(71\)80282-8](https://doi.org/10.1016/0009-2614(71)80282-8), 1971.
- 747 Ferguson, J. and Fielding, P. E.: The origins of the colors of natural yellow, blue, and green sapphires,
748 *Aust. J. Chem.*, 25, 1371–1385, <https://doi.org/10.1071/CH9721371>, 1972.
- 749 Filatova, N. V., Kosenko, N. F., and Artyushin, A. S.: The physicochemical analysis of bayerite Al(OH)₃
750 → γ -Al₂O₃ transformation, *J. Sib. Fed. Univ. Chem.*, 14, 527–538,
751 <https://doi.org/10.17516/1998-2836-0260>, 2021.
- 752 Fritsch, E., Chalain, J. P., Hanni, H., Devouard, B., Chazot, G., Giuliani, G., Schwartz, D., Rollion-Bard,
753 C., Garnier, V., Barda, S., Ohnenstetter, D., Notari, F., and Maitrallet, P.: Le nouveau traitement
754 produisant des couleurs orange a jaune dans les saphirs, *Revue de Gemmologie* n° 147–Février
755 2003, 147, 11–23, 2003.

- 756 Gog, H. V.: First principles study of dehydration interfaces between diaspore and corundum, gibbsite and
757 boehmite, and boehmite and γ - Al_2O_3 : Energetic stability, interface charge effects, and dehydration
758 defects, *Appl. Surf. Sci.*, 541, 148501, <https://doi.org/10.1016/j.apsusc.2020.148501>, 2021.
- 759 Häger, T.: Farbgebende und "farbhemmende" Spurenelemente in blauen Saphiren, *Berichte der*
760 *Deutschen Mineralogischen Gesellschaft* – Beih. Eur. J. Mineral., 4, 109, 1992.
- 761 Häger, T.: High temperature treatment of natural corundum, in: *Proceeding of the International Workshop*
762 *on Material Characterization by Solid State Spectroscopy: The Minerals of Vietnam, Hanoi*, 4–10
763 April 2001, 1–10, 2001.
- 764 Hughes, E. B. and Perkins, R.: Madagascar sapphire: Low temperature heat treatment experiments, *Gems*
765 *Gemol.*, 55, 184–197, <http://doi.org/10.5741/GEMS.55.2.184>, 2019.
- 766 Hughes, R. W. (1st edn.): *Ruby & Sapphire*, RWH Publishing, 511 pp., ISBN 0964509768, 1997.
- 767 Hughes, R. W.: *Ruby & sapphire: A gemologist's guide*, RWH Publishing/Lotus Publishing, 816 pp.,
768 ISBN 9780964509719, 2017.
- 769 Jaliya, R. G. C., Dharmaratne, P. G. R., and Wijesekara, K. B.: Characterization of heat treated geuda
770 gemstones for different furnace conditions using FTIR, XRD and UV–Visible spectroscopy
771 methods, *Solid Earth Sci.*, 5, 282–289, <https://doi.org/10.1016/j.sesci.2020.11.001>, 2020.
- 772 Jung, I. H., Eriksson, G., Wu, P., and Pelton, A.: Thermodynamic modeling of the Al_2O_3 – Ti_2O_3 – TiO_2
773 system and its applications to the Fe–Al–Ti–O inclusion diagram, *ISIJ INT.*, 49, 1290–1297,
774 <https://doi.org/10.2355/isijinternational.49.1290>, 2009.
- 775 Kammerling, R. C., Koivular, J. I., and Kane, R. E.: Gemstone enhancement and its detection in the
776 1980s, *Gems Gemol.*, 26, 32–49, <https://doi.org/10.5741/GEMS.26.1.32>, 1990.
- 777 Kane, R. E.: The gemological properties of Chatham flux–grown synthetic orange sapphire and synthetic
778 blue sapphire, *Gems Gemol.*, 18, 140–153, <https://doi.org/10.5741/GEMS.18.3.140>, 1982.
- 779 Klopogge, J. T., Ruan, H. D. and Frost, R. L.: Thermal decomposition of bauxite minerals: infrared
780 emission spectroscopy of gibbsite, boehmite and diaspore, *J. Mater. Sci.*, 37, 1121–1129,
781 <https://doi.org/10.1023/A:1014303119055>, 2002.
- 782 Krebs, J. J. and Maisch, W. G.: Exchange effects in the optical–absorption spectrum of Fe^{3+} in Al_2O_3 ,
783 *Phys. Rev. B*, 4, 757–769, <https://doi.org/10.1103/PhysRevB.4.757>, 1971.
- 784 Kyi, U. H., Buchhol, P., and Wolf, D.: Heat treatment of milky sapphires from the Mogok stone tract,
785 Myanmar, *J. Gemmol.*, 26, 313–315, <https://doi.org/10.15506/jog.1999.26.5.313>, 1999.
- 786 Lacovara, P., Esterowitz, L., and Kokta, M.: Growth, spectroscopy, and lasing of titanium–doped
787 sapphire, *IEEE J. Quantum Electron.*, 21, 1614–1618, <https://doi.org/10.1109/JQE.1985.1072563>,
788 1985.
- 789 Mattson, S. M. and Rossman, G. R.: Fe^{2+} – Ti^{4+} charge transfer in stoichiometric Fe^{2+} , Ti^{4+} –minerals, *Phys.*
790 *Chem. Miner.*, 16, 78–82, <https://doi.org/10.1007/BF00201333>, 1988.
- 791 McClure, D. S.: Optical spectra of transition–metal ions in corundum, *J. Chem. Phys.*, 36, 2757–2779,
792 <https://doi.org/10.1063/1.1732364>, 1962.

- 793 McClure, S. F. and Smith, C. P.: Gemstone enhancement and detection in the 1990s, *Gems Gemol.*, 36,
794 336–539, <http://doi.org/10.5741/GEMS.36.4.336>, 2000.
- 795 McClure, S. F., Kane, R. E., and Sturman, N.: Gemstone enhancement and detection in the 2000s, *Gems*
796 *Gemol.*, 46, 218–240, <http://doi.org/10.5741/GEMS.46.3.218>, 2010.
- 797 Mikhailik, V. B., Kraus, H., Wahl, D., and Mykhaylyk, M. S.: Luminescence studies of Ti-doped Al₂O₃
798 using vacuum ultraviolet synchrotron radiation., *Appl. Phys. Lett.*, 86, 101909,
799 <http://doi.org/10.1063/1.1880451>, 2005.
- 800 Monarumit, N., Lhuaamporn, T., Wathanakul, P., Saiyasombat, C., and Wongkokua, W.: The acceptor-
801 donor pair recombination of beryllium-treated sapphires, *Radiat. Phys. Chem.*, 206, 110756,
802 <https://doi.org/10.1016/j.radphyschem.2023.110756>, 2023.
- 803 Moon, A. R. and Phillips, M. R.: Defect clustering and color in Fe,Ti: α -Al₂O₃, *J. Am. Ceram. Soc.*, 77,
804 356–367, <https://doi.org/10.1111/j.1151-2916.1994.tb07003.x>, 1994.
- 805 [Nasdala, L., and Fritsch, E.: Luminescence: The “Cold Glow” of Minerals, *Elements*, 20, 287–292.](https://doi.org/10.2138/gselements.20.5.287)
806 <https://doi.org/10.2138/gselements.20.5.287>, 2024.
- 807 Nassau, K.: The causes of color, *Sci. Am.*, 243, 124–154,
808 <https://doi.org/10.1038/SCIENTIFICAMERICAN1080-124>, 1980.
- 809 Nassau, K.: Heat treating ruby and sapphire: Technical aspects, *Gems Gemol.*, 17, 121–131,
810 <https://doi.org/10.5741/GEMS.17.3.121>, 1981.
- 811 Nelson, D. F. and Sturge, M. D.: Relation between absorption and emission in the region of the R lines of
812 ruby, *Phys. Rev.*, 137, A1117–A1130, <https://doi.org/10.1103/PhysRev.137.A1117>, 1965.
- 813 Nikolskaya, L. V., Terekhova, V. M., and Samoilovich, M. I.: On the origin of natural sapphire color,
814 *Phys. Chem. Miner.*, 3, 213–224, <https://doi.org/10.1007/BF00633571>, 1978.
- 815 Norrbo, I., Gluchowski, P., Hyppänen, I., Laihininen, T., Laukkanen, P., Mäkelä, J., Mamedov, F., Santos,
816 H. S., Sinkkonen, J., Tuomisto, M., Viinikanoja, A., and Lastusaari, M.: Mechanisms of
817 tenebrescence and persistent luminescence in synthetic hackmanite Na₈Al₆Si₆O₂₄(Cl,S)₂, *ACS*
818 *Appl. Mater. Interfaces*, 8, 11592–11602, <https://doi.org/10.1021/acsami.6b01959>, 2016.
- 819 Notari, F., Fritsch, E., and Grobon, C.: Comment l'observation de la luminescence (fluorescence) peut
820 aider à l'identification des corindons jaunes, rose orange et orange, traités par diffusion du
821 beryllium (How the observation of luminescence might aid in the identification of yellow, orangy
822 pink and orange corundum treated by Be-diffusion), *Rev. de Gem.*, 148, 40–43, 2003.
- 823 Notari, F., Hainschwang, T., Caplan, C., and Ho, K.: The heat treatment of corundum at moderate
824 temperature, *InColor*, 42, 15–23, 2018.
- 825 Page, P. S., Dhabekar, B. S., Bhatt, B. C., Dhoble, A. R., and Godbole, S. V.: Role of Ti⁴⁺ in the
826 luminescence process of Al₂O₃:Si,Ti, *J. Lumin.*, 130, 882–887,
827 <https://doi.org/10.1016/j.jlumin.2009.12.029>, 2010.
- 828 Palanza, V., Di Martino, D., Paleari, A., Spinolo, G., and Loredana, P.: Micro-Raman spectroscopy
829 applied to the study of inclusions within sapphire, *J. Raman Spectrosc.*, 39, 1007–1011,
830 <https://doi.org/10.1002/jrs.1939>, 2008.

- 831 Palke, A. C., Saeseaw, S., Renfro, N. D., Sun, Z., and McClure, S. F.: Geographic origin determination of
832 blue sapphire, *Gems Gemol.*, 55, 536–579, <https://doi.org/10.5741/gems.55.4.536>, 2019.
- 833 Peiris, B. P. S.: Color enhancement of diesel geuda, in: Proceedings of the National symposium on geuda
834 heat treatment, Sri Lanka, 10–11 June 1993, 113–122, 1993.
- 835 Perera, S. Z., Pannila, A. S., Gunasekera, H. P. N. J., and Ediriweera, R. N.: Anomalous behaviour of
836 certain geuda corundums during heat treatment, *J. Gemmol.*, 22, 405–407,
837 <https://doi.org/10.15506/jog.1991.22.7.405>, 1991.
- 838 Perera, I.: Identification of treatable geuda by spectral investigations, in: Proceedings of the National
839 symposium on geuda heat treatment, Sri Lanka, 10–11 June 1993, 89–98, 1993
- 840 Pisutha–Armond, V.: Ruby & sapphire treatments and identification: Decades of advancement, Amarin
841 Printing and Publishing, Bangkok, 96 pp., ISBN 978–6169145097, 2017.
- 842 Saeseaw, S., Kongsomart, B., Atikarnsakul, U., Khowpong, C., Verriest, W., and Soonthorntantikul, W.:
843 Update on “low temperature” heat treatment of Mozambican ruby: A focus on inclusions and
844 FTIR spectroscopy. News from research, Gemological Institute of America, 37 pp., 2018.
- 845 [Saeseaw, S., Khowpong, C., and Verriest, W.: Low temperature heat treatment of pink sapphires from
846 Hakaka, Madagascar, *Gems Gemol.*, 56, 448–457, <http://doi.org/10.5741/GEMS.56.4.448>, 2020.](#)
- 847 [Samadhi, T., Subagjo, S., Lismana, K., and Fuadi, K.: Synthesis of \$\gamma\$ -Al₂O₃ catalyst support from kaolin
848 of Indonesian origin. *ITB J. Eng. Sci.*, 43, 113–126,
849 <https://dx.doi.org/10.5614/itbj.eng.sci.2011.43.2.3>, 2011.](#)
- 850 Schmetzer, K. and Kiefert, L.: Spectroscopic evidence for heat treatment of blue sapphires from Sri
851 Lanka—additional data, *J. Gemmol.*, 22, 80–82, 1990.
- 852 Segura, O.: La luminescence orange des corindons, Diplome Universitaire de Gemmologie de Nantes, 60
853 pp., 2013.
- 854 [Sifontes, Á. B., Ávila, E., Gutiérrez, B., Rengifo, M., Mónaco, A., Díaz, Y., and Llovera, L.: Relevant
855 aspects of the biosynthesis of porous aluminas using glycosides and carbohydrates as biological
856 templates, *Biotechnol. Res. Innov.*, 3, 22–37, <https://doi.org/10.1016/j.biori.2019.01.004>, 2019.](#)
- 857 Smith, C. P.: A contribution to understanding the infrared spectra of rubies from Mong Hsu, Myanmar, *J.*
858 *Gemmol.*, 24, 321–335, <http://doi.org/10.15506/JoG.1995.24.5.321>, 1995.
- 859 Soonthorntantikul, W., Khowpong, C., Atikarnsakul, U., Saeseaw, S., Sangsawong, S., Verriest, W., and
860 Palke, A.: Observations on the heat treatment of basalt–related blue sapphires. News from
861 research, Gemological Institute of America, 60 pp., 2019.
- 862 Soonthorntantikul, W., Atikarnsakul, U., and Verriest, W.: Blue sapphires from Mogok, Myanmar: A
863 gemological review, *Gems Gemol.*, 57, 292–317, <https://doi.org/10.5741/GEMS.57.4.292>, 2021.
- 864 Soysa, E. S. K. and Fernando, W. S.: A field classification of low value corundum in Sri Lanka, *J. Natn.*
865 *Sci. Coun. Sri Lanka*, 20, 51–57, <https://doi.org/10.4038/jnsfsr.v20i1.8058>, 1992.
- 866 Spencer, L. J.: South African occurrences of willemite. Fluorescence of willemite and some other zinc
867 minerals in ultra–violet rays, *Mineral. Mag.*, 21, 388–396,
868 <https://doi.org/10.1180/minmag.1927.021.119.04>, 1927.

- 869 Sripoonjan, T., Lhuaamporn, T., Nilhud, N., Sukkee, N., and Sutthirat, C.: Characteristics of Cyangugu
870 sapphire from rwanda, in: Proceedings of the 4th international gem and jewelry conference
871 (GIT2014) Chiang Mai, Thailand, 165–168, 2014.
- 872 Strange, L., Zhang, Y., Son, J., Gao, J., Joshi, V., and Yu, X. Y.: Aluminum hydroxide, bayerite,
873 boehmite, and gibbsite ToF–SIMS spectra in the negative ion mode. I. Surf. Sci. Spectra, 29,
874 025001. <https://doi.org/10.1116/6.0001935>, 2022.
- 875 Sun, T., Zhuo, Q., Chen, Y., and Wu, Z.: Synthesis of boehmite and its effect on flame retardancy of
876 epoxy resin, High Perform. Polym., 27, 1, 100–104, <https://doi.org/10.1177/0954008314540312>,
877 2015.
- 878 Sutthirat, C., Pattamalai, K., Sakkaravej, S., Pumpeng, S., Pisutha–Arnond, V., Wathanakul, P., Atichat,
879 W., and Sriprasert, B.: Indications of heating in corundum from experimental results, Gems
880 Gemol., 42, 86, 2006.
- 881 Themelis, T. (3rd edn.): The heat treatment of ruby & sapphire: Experiments & observations, Ted
882 Themelis, 294 pp., ISBN 0940965577, 2018.
- 883 Townsend, M. G.: Visible charge transfer band in blue sapphire, Solid State Commun., 6, 81–83,
884 [https://doi.org/10.1016/0038-1098\(68\)90005-7](https://doi.org/10.1016/0038-1098(68)90005-7), 1968.
- 885 [Vertriest, W., Palke, A. C., and Renfro, N. D.: Field Gemology: Building a Research Collection and
886 Understanding the Development of Gem Deposits, Gems Gemol., 55, 491–494, 2019,
887 <https://dx.doi.org/10.5741/GEMS.55.4.490>](https://dx.doi.org/10.5741/GEMS.55.4.490)
- 888 Vigier, M. and Fritsch, E.: More on orange luminescence in corundum, Gems Gemol., 58, 376–377,
889 2022.
- 890 Vigier, M., Fritsch, E., and Segura, O.: Orange luminescence of corundum as a source of geologic
891 information?, Goldschmidt 2021 Abstract, Virtual conference, 4–9 July 2021,
892 <https://doi.org/10.7185/gold2021.3467>, 2021a.
- 893 Vigier, M., Fritsch, E., and Segura, O.: Orange luminescence of corundum an atypical origin for
894 gemmologists (part one), Revue de L'Association Française de Gemmologie N° 211–Mars 2021,
895 12–19, 2021b.
- 896 Vigier, M., Fritsch, E., and Segura, O.: Orange luminescence of corundum an atypical origin for
897 gemmologists (part two), Revue de L'Association Française de Gemmologie N° 212–Juin 2021,
898 13–19, 2021c.
- 899 Vigier, M., Fritsch, E., Cavignac, T., Latouche, C., and Jobic, S.: Shortwave UV blue luminescence of
900 some minerals and gems due to titanate groups, Minerals, 13, 104,
901 <https://doi.org/10.3390/min13010104>, 2023.
- 902 [Vlaskin, M. S., Grigorenko, A. V., Zhuk, A. Z., Lisitsyn, A. V., Sheindlin, A. E., and Shkol'nikov, E. I.:
903 Synthesis of high purity \$\alpha\$ -Al₂O₃ from boehmite obtained by hydrothermal oxidation of aluminum,
904 High Temp., 54, 322–329, <https://doi.org/10.1134/S0018151X16020231>, 2016.](https://doi.org/10.1134/S0018151X16020231)
- 905 Webster, R. (6th edn.): Practical gemmology. A study of the identification of gemstones, pearls, and
906 ornamental minerals, N.A.G. Press, Suffolk, USA, 92 pp., 1984.

- 907 Wong, W. C., McClure, D. S., Basun, S. A., and Kokta, M. R.: Charge-exchange processes in titanium-
908 doped sapphire crystals. I. Charge-exchange energies and titanium-bound excitons, *Phys. Rev. B*
909 *Condens. Matter*, 51, 5682-5692, <https://doi.org/10.1103/physrevb.51.5682>, 1995a.
- 910 Wong, W. C., McClure, D. S., Basun, S. A., and Kokta, M. R.: Charge-exchange processes in titanium-
911 doped sapphire crystals. II. Charge-transfer transition states, carrier trapping, and detrapping,
912 *Phys. Rev. B Condens. Matter*, 51, 5693-5698, <https://doi.org/10.1103/physrevb.51.5693>, 1995b.
- 913 Zeug, M., Nasdala, L., Wanthanachaisaeng, B., Balmer, W.A., Corfu, F., and Wildner, M.: Blue zircon
914 from Ratanakiri, Cambodia, *J. Gemmol.*, 36, 112-132,
915 <http://dx.doi.org/10.15506/JoG.2018.36.2.112>, 2018.
- 916 Zeug, M., Nasdala, L., Chanmuang N., C., and Hauzenberger, C.: Gem topaz from the Schneckenstein
917 crag, Saxony, Germany: Mineralogical characterization and luminescence, *Gems Gemol.*, 58, 2-
918 17, <https://doi.org/10.5741/GEMS.58.1.2>, 2022.